Interaction of waves with frictional interfaces using summation-by-parts difference operators, 2. Extension to full elastodynamics

Jeremy E. Kozdon[*,a], Eric M. Dunham[a], Jan Nordström[b,c]

[a] *Department of Geophysics, Stanford University, 397 Panama Mall, Stanford, CA 94305, USA*
[b] *Department of Information Technology, Uppsala University, Box 337, SE-75105 Uppsala, Sweden*
[c] *Department of Aeronautics and Systems Integration, FOI, The Swedish Defence Research Agency, SE-164 90 Stockholm, Sweden*

Abstract

In this work we extend Part 1 [Interaction of waves with frictional interfaces using summation-by-parts difference operators, 1. Weak enforcement of nonlinear boundary conditions; Jeremy E. Kozdon, Eric M. Dunham, and Jan Nordström, submitted to J. Comp. Phys.] to the full governing equations of elastodynamics, which describe multidirectional deformation carried by a dilatational wave and two shear waves with orthogonal polarizations. As in Part 1, we only consider 1-D problems, but generalize the analysis to the case of an internal interface (or fault) that separates two elastic bodies with differing material properties. The fault strength is governed by a nonlinear function of sliding velocity and a set of internal state variables obeying differential evolution equations (a mathematical framework known as rate-and-state friction). The method is based on summation-by-parts finite difference operators and weak enforcement of boundary conditions using the simultaneous approximation term method. We prove that the method is strictly stable and dissipates energy at a slightly faster rate than the continuous solution (with the difference in energy dissipation rates vanishing as the mesh is refined).

Two test problems, one which permits a steady state sliding solution and another that does not, demonstrate the stability and accuracy of the method.

1. Introduction

In the companion study to this work [Interaction of waves with frictional interfaces using summation-by-parts difference operators, 1. Weak enforcement of nonlinear boundary conditions; Jeremy E. Kozdon, Eric M. Dunham, and Jan Nordström, submitted to J. Comp. Phys.], hereafter referred to as Part 1, we developed a strictly stable numerical method for sliding of an elastic material on a rigid substrate, with the interfacial friction law taking the form of a nonlinear boundary condition. That was done for the special case of unidirectional deformation. In this work, we extend the method in three ways. We generalize to multidirectional deformation described by the full set of the elastodynamic equations (tensor elasticity), faults that separate elastic bodies with different material properties (two-sided faults), and rate-and-state friction laws that capture the dependence of fault strength on the past sliding history.

Since earthquakes and other frictional contact problems are inherently boundary driven, numerical errors and instabilities that arise due to the treatment of the frictional interfaces can destroy the accuracy of the solution. This includes ground motion predictions which are critical for seismic hazard assessment. As was demonstrated in Part 1, these errors can be particularly damaging to the solution when long time integration is required and a method which is not strictly stable is used. Throughout this paper we use the term boundary to not only refer to "outer" boundaries, either physical or computational, but also to internal frictional interfaces, across which fields may be discontinuous.

In this paper we develop a numerical method that can be applied to problems of propagating shear ruptures, particularly those arising in earthquake dynamics. The rupture problem couples seismic wave propagation and frictional sliding on faults, and is thus influenced by both fault and surrounding material response. Over the temporal and spatial scales of interest in rupture dynamics, the rock response can be approximated as linear elastic (though more realistic models can be considered which account for inelastic deformation) and the fault as an infinitesimally thin frictional interface. As the material on one side of the fault is displaced with respect to the other (with the discontinuity in displacement referred to as slip), jump conditions, arising from friction laws and force balance considerations, relate stress and velocity on the two sides of the fault. Friction laws are constitutive relations

*Corresponding Author
Email address: jkozdon@stanford.edu (Jeremy E. Kozdon)

which depend not only on the current slip velocity and tractions acting on the fault but also, for instance, the history of sliding, frictional heat generation, and transport of heat and pore fluids in the fault zone. The latter processes are parameterized in terms of "state variables" that obey differential evolution equations which are distinct from the governing equations of the elastic medium.

A widely used mathematical framework known as rate-and-state friction captures many features observed in laboratory friction experiments [Dieterich, 1979, Rice, 1983, Ruina, 1983, Rice and Ruina, 1983, Marone, 1998, Rice et al., 2001]. The fault shear strength τ (resistance to slip) is

$$\tau = \sigma_n f(V, \Psi), \tag{1}$$

where σ_n is the normal stress acting on the fault (taken to be positive in compression), and the friction coefficient f depends on the slip velocity, V, and a state variable, Ψ, that obeys the evolution law

$$\frac{d\Psi}{dt} = G(V, \Psi), \tag{2}$$

Under conditions of steady sliding at constant velocity V, the state variable evolves toward $\psi_{ss}(V)$, defined implicitly through

$$0 = G(V, \psi_{ss}(V)), \tag{3}$$

and the friction coefficient approaches its steady state friction value, $f_{ss}(V)$:

$$f_{ss}(V) = f(V, \psi_{ss}(V)). \tag{4}$$

A widely used state evolution law is the slip law [Rice, 1983]:

$$G(V, \psi(V)) = -\frac{V}{L}\left[f(V, \Psi) - f_{ss}(V)\right], \tag{5}$$

which describes evolution of f toward $f_{ss}(V)$ over the state evolution distance L.

The steady state velocity dependence may be either velocity-strengthening ($f'_{ss}(V) > 0$) or velocity-weakening ($f'_{ss}(V) < 0$). Velocity-weakening interfaces between prestressed elastic solids are prone to instability, in that the release of strain energy from the elastic medium in response to slip drives the interface to faster slip rates, which further weakens the interface, causing even more rapid sliding.

Experiments in which a sudden change from steady sliding at velocity V to $V + \Delta V$ is imposed (velocity stepping tests) reveal an even richer

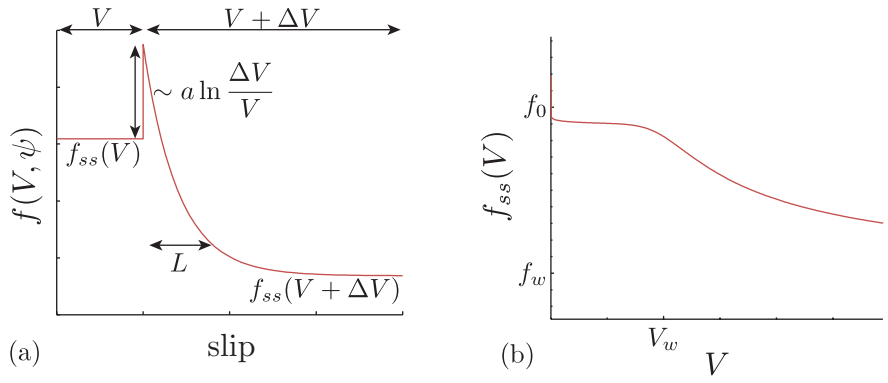

Figure 1: (a) Response of the friction coefficient, f, to an abrupt increase in slip velocity from V to $V + \Delta V$. The instantaneous increase in f, known as the direct effect, is followed by evolution over the state evolution distance, L, to the new, lower steady state friction coefficient. (b) Steady state friction coefficient that drops from f_0 at slow speeds toward the fully weakened value f_w when V surpasses the weakening velocity V_w.

behavior, as illustrated in Figure 1(a). Rather than abruptly changing from $f_{ss}(V)$ to $f_{ss}(V + \Delta V)$, f first jumps to a new value (different from $f_{ss}(V + \Delta V)$) and then evolves with slip to the new steady state $f_{ss}(V + \Delta V)$. The instantaneous change in f is known as the direct effect, and is quantified by the parameter

$$a = V \frac{\partial f(V, \Psi)}{\partial V}, \tag{6}$$

which is $\sim$0.01 for a wide range of materials. Both velocity stepping experiments and theoretical considerations (of how sliding is accommodated at the microscopic scale through the thermally activated motion of defects at highly stressed contacts bridging the interface [Rice et al., 2001]) show that $a > 0$. This means that the interface is always instantaneously velocity-strengthening, which is a sufficient condition for well-posedness of frictional sliding between elastic bodies, as discussed in Part 1 and also in Rice et al. [2001].

The steady state friction law used in this work is shown in Figure 1(b) and exhibits the extreme velocity weakening behavior that has been observed in numerous high speed friction experiments; the specific forms of the equations used in this work are discussed in more detail in Sec. 2.1.

An alternative, commonly used class of friction laws are slip-weakening laws, for which the friction coefficient depends only on the cumulative slip [Andrews, 1976, Ida, 1972, Palmer and Rice, 1973]. Such models also feature an on/off behavior, in that the fault does not slip when shear stress is less than the fault strength (in contrast to rate-and-state friction laws, for which shear stress and fault strength are always identical). In the most commonly used slip-weakening law, the friction coefficient decreases from the static friction coefficient to the dynamic friction coefficient over a characteristic slip distance. The on/off behavior leads to non-smooth solutions in the medium, which can degrade the accuracy of the numerical methods.

However, all of our conclusions regarding well-posedness of the continuous problem and stability of the numerical method developed in this work for rate-and-state friction laws apply also for slip-weakening friction laws. This is because during sliding, the slip-weakening law can be considered to be a particular case of (1), with Ψ interpreted as the cumulative slip distance, such that $G(V, \Psi) = |V|$, and the friction coefficient depending only on slip: $f(V, \Psi) = f(\Psi)$. Despite the popularity of slip-weakening laws in modeling earthquake ruptures, the full rate-and-state framework is required to explain laboratory friction experiments.

More generally $\tau = F(V, \Psi, \sigma_n)$ which allows for a more complex dependence on σ_n that arises in some physical models [Nielsen et al., 2008]. Since earthquake problems are boundary driven, accurate handling of these highly nonlinear friction laws governing the fault is critical for robust and reliable simulation.

Before outlining the approach taken in this work, we briefly outline previous work for modeling earthquake ruptures. The boundary integral equation method (BIEM) has been quite popular for the study of many crack and rupture propagation problems [Das, 1980, Andrews, 1985, Das and Kostrov, 1988, Cochard and Madariaga, 1994, Perrin et al., 1995, Geubelle and Rice, 1995, Kame and Yamashita, 1999, Aochi et al., 2000, Lapusta et al., 2000, Day et al., 2005, Noda et al., 2009]. BIEM reduces the problem to solving only for the solution along the fault and the material response enters through the need to compute convolutions over the past history of slip or tractions on that fault. The main computational cost associated with the method is the computation of the convolutions. The big drawback of the BIEM is that it only works for a linear elastic medium with uniform material properties.

Finite element methods (FEM) overcome some of these computational challenges, and have been successfully applied to rupture problems [Oglesby et al., 1998, Aagaard et al., 2001, Ma and Liu, 2006, Moczo et al., 2007]. The meshes for these methods can be quite general and typically lower order

elements are used. The drawbacks of traditional FEM are nondiagonal mass matrices. Solving the resulting linear system can be avoided by lumping the mass matrix, though this makes the spatial difference operator rank-deficient, leading to non-physical oscillations (hourglass modes) that must be damped. To address this the use of high-order methods, such as spectral-element methods [Ampuero, 2002, Festa and Vilotte, 2005, Kaneko et al., 2008], which have diagonal mass matrices due to the choice of basis functions and quadrature points, and discontinuous Galerkin methods [de la Puente et al., 2009] are gaining in popularity.

Finite difference methods, especially those on staggered grids, are also commonly used [Andrews, 1976, Miyatake, 1980, Day, 1982, Madariaga et al., 1998, Day et al., 2005, Moczo et al., 2007]. These methods are very efficient for wave propagation, but proving stability is difficult when using the methods with nonlinear boundary conditions [Rojas et al., 2009].

We note that to date, none of the methods above have demonstrated higher-order (greater than second order) convergence, even for smooth problems with nonlinear boundary conditions.

Here, as in Part 1, we use summation-by-parts (SBP) finite difference methods [Kreiss and Scherer, 1974, 1977, Strand, 1994, Carpenter et al., 1999, Mattsson and Nordström, 2004] on an unstaggered grid. An SBP difference approximation to the first derivative has the form

$$\frac{\partial v}{\partial y} \approx \boldsymbol{H}^{-1}\boldsymbol{Q}\,\boldsymbol{v}, \tag{7}$$

where $\boldsymbol{H}$ is a symmetric positive definite matrix, $\boldsymbol{Q}$ is an almost skew-symmetric matrix with $\boldsymbol{Q}^T + \boldsymbol{Q} = \mathbf{diag}(-1, 0, \ldots, 0, 1)$, and the vector $\boldsymbol{v} = (v_0, v_1, \ldots, v_N)^T$ is the grid data. These are called SBP methods because they mimic integration-by-parts properties of the continuous problem. Defining the continuous and discrete norms

$$(u, v) = \int_a^b u(y)\; v(y)\; dy \quad \text{and} \quad (\boldsymbol{u}, \boldsymbol{v})_h = \boldsymbol{u}^T\; \boldsymbol{H}\boldsymbol{v}, \tag{8}$$

this becomes clear since

$$\left(v, \frac{dv}{dy}\right) = \int_a^b v\; \frac{dv}{dy}\; dy = \frac{1}{2}\left[v(b)^2 - v(a)^2\right], \tag{9}$$

$$(\boldsymbol{v}, \boldsymbol{H}^{-1}\boldsymbol{Q}\boldsymbol{v})_h = \boldsymbol{v}^T\; \boldsymbol{Q}\; \boldsymbol{v} = \frac{1}{2}\boldsymbol{v}^T\; (\boldsymbol{Q} + \boldsymbol{Q}^T)\; \boldsymbol{v} = \frac{1}{2}(v_N^2 - v_0^2). \tag{10}$$

SBP operators are basically standard central difference methods, having orders $q = 2, 4, 6, 8, \ldots$ in the interior, that become one-sided methods

near boundaries in a manner that maintains the SBP property. The boundary order of accuracy r is typically lower than the interior accuracy q and hence the global accuracy is $p = r + 1$ [Gustafsson, 1975, Svärd and Nordström, 2007]. In this work we only consider diagonal norm (diagonal $\boldsymbol{H}$) operators which have interior accuracy $q = 2s$ ($s = 1, 2, \dots$), boundary accuracy $r = s$, and global accuracy $p = s + 1$. There are SBP operators that have boundary accuracy $r = 2s - 1$ and global accuracy $p = 2s$, but using these makes proving stability difficult for problems with variable coefficients and/or coordinate transforms [Nordström and Carpenter, 2001, Olsson, 1995, Nordström, 2006].

Using SBP difference methods alone is not enough to ensure a stable method and appropriate boundary treatment is needed. Though there are many ways to incorporate boundary conditions, here we exclusively use weak enforcement of the boundary conditions through the simultaneous approximation term (SAT) method [Carpenter et al., 1994]. One of the main advantage of this method is that it is strictly stable [Gustafsson et al., 1996], meaning that the numerical method dissipates energy slightly faster than the continuous solution (difference in the rates goes to zero as the mesh is refined). Strict stability can shown to lead to error bounds in time; see Nordström [2007] and the references therein. If strong enforcement of the boundary conditions, known as the injection method, is used nothing can be said about the energy dissipation rate of the method and the method can lead to energy growth in the solution with long time integration; this was demonstrated for frictional sliding problems in Part 1.

One of the most important results from Part 1 concerned the stiffness of the system of ODEs resulting from the discretization of the governing equations with the inclusion of the boundary conditions. Namely, it was shown that unless the nonlinear boundary conditions are formulated in terms of the characteristic variables, the resulting system of equations can be arbitrarily stiff, meaning that efficient explicit time integration is not possible for certain portions of the parameter space.

The remainder of the paper is as follows: In Sec. 2 the continuous problem involving tensor elasticity with a two-sided fault and differing material properties is introduced and well-posedness is established. A strictly stable discretization of this problem is derived in Sec. 3 using SBP difference operators and the SAT method for incorporating boundary conditions. Numerical examples confirm the theoretical results in Sec. 4 and conclusions are drawn in Sec. 5.

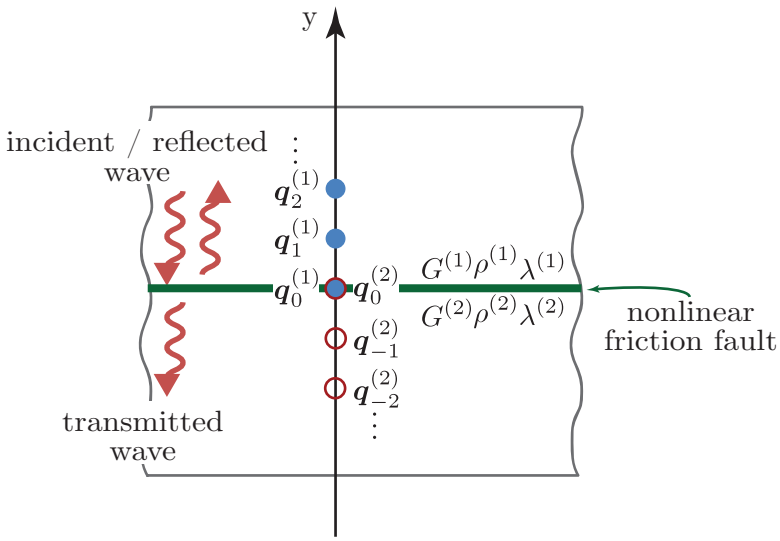

Figure 2: Material properties are allowed to differ on both sides of the fault, as indicated by superscript (l). The two grid points on the fault ($\boldsymbol{q}_0^{(1)}$ and $\boldsymbol{q}_0^{(2)}$) are collocated in order to accommodate discontinuities in velocity and stress across the fault.

2. Continuous Problem

Consider a two-sided fault system (Figure 2) where the material properties on the two sides of the fault ($y = 0$) can differ, as indicated in the figure by $\rho^{(l)}$ (density), $G^{(l)}$ (shear modulus), and $\lambda^{(l)}$ (Lamé's first parameter) where $l = 1$ refers to $y > 0$ and $l = 2$ to $y < 0$. We consider the most general case of three components of particle velocity, two of which are tangential to the fault (v_x and v_z) and one of which is normal to the fault (v_y). The stress tensor is symmetric ($\sigma_{ij} = \sigma_{ji}$); hence, there are only six, and not nine, components of stress to consider. Two components exert shear tractions on the fault (σ_{yx} and σ_{yz}) and one component exerts a normal traction on the fault (σ_{yy}); the other three components of stress (σ_{xx}, σ_{zz}, and σ_{xz}) do not exert tractions on the fault with this problem configuration.

The governing equations of linear elasticity are

$$\rho^{(l)} \frac{\partial v_i}{\partial t} = \frac{\partial \sigma_{ki}}{\partial x_k}, \qquad i = x, y, z, \tag{11}$$

$$\frac{\partial \sigma_{ij}}{\partial t} = \lambda^{(l)} \, \delta_{ij} \frac{\partial v_k}{\partial x_k} + G^{(l)} \left(\frac{\partial v_i}{\partial x_j} + \frac{\partial v_j}{\partial x_i} \right), \quad i, j = x, y, z, \tag{12}$$

where here, as in subsequent equations, summation is implied over $\{x, y, z\}$ for repeated subscript indices and the physical parameters $\rho^{(l)}$, $G^{(l)}$, and $\lambda^{(l)}$ are taken to be constants on either side of the fault. It is well known that (11) and (12) admit three wave types, two transverse waves polarized in the x- and z-directions (we will only consider the 1-D problem in the y-direction), known as shear or S-waves, and a single longitudinal wave polarized in the y-direction, known as the dilatational or P-wave. By introducing a change of variables and considering only the 1-D problem in the y-direction, the governing equations can be written as a symmetric first order, hyperbolic

system:

$$\frac{\partial \boldsymbol{q}^{(l)}}{\partial t} = \boldsymbol{A}^{(l)} \frac{\partial \boldsymbol{q}^{(l)}}{\partial y}, \tag{13}$$

$$\boldsymbol{q}^{(l)} = \frac{1}{\sqrt{2\rho^{(l)}}} \begin{bmatrix} \rho^{(l)}\, v_x \\ \rho^{(l)}\, v_y \\ \rho^{(l)}\, v_z \\ \sqrt{2} s_{xx}/(2c_s^{(l)}) + \sigma_m/c_p^{(l)} \\ \sqrt{2} s_{yy}/(2c_s^{(l)}) + \sigma_m/c_p^{(l)} \\ \sqrt{2} s_{zz}/(2c_s^{(l)}) + \sigma_m/c_p^{(l)} \\ \sigma_{yx}/c_s^{(l)} \\ \sigma_{xz}/c_s^{(l)} \\ \sigma_{yz}/c_s^{(l)} \end{bmatrix}, \tag{14}$$

$$\sigma_m = \frac{1}{3}\left(\sigma_{xx} + \sigma_{yy} + \sigma_{zz}\right), \tag{15}$$

$$s_{ij} = \sigma_{ij} - \sigma_m \delta_{ij}, \tag{16}$$

$$\boldsymbol{A}^{(l)} = \begin{bmatrix} 0 & 0 & 0 & 0 & 0 & 0 & c_s^{(l)} & 0 & 0 \\ 0 & 0 & 0 & a_1^{(l)} & a_2^{(l)} & a_1^{(l)} & 0 & 0 & 0 \\ 0 & 0 & 0 & 0 & 0 & 0 & 0 & 0 & c_s^{(l)} \\ 0 & a_1^{(l)} & 0 & 0 & 0 & 0 & 0 & 0 & 0 \\ 0 & a_2^{(l)} & 0 & 0 & 0 & 0 & 0 & 0 & 0 \\ 0 & a_1^{(l)} & 0 & 0 & 0 & 0 & 0 & 0 & 0 \\ c_s^{(l)} & 0 & 0 & 0 & 0 & 0 & 0 & 0 & 0 \\ 0 & 0 & 0 & 0 & 0 & 0 & 0 & 0 & 0 \\ 0 & 0 & c_s^{(l)} & 0 & 0 & 0 & 0 & 0 & 0 \end{bmatrix}, \tag{17}$$

$$a_1^{(l)} = \frac{1}{3}\left(c_p^{(l)} - \sqrt{2} c_s^{(l)}\right), \tag{18}$$

$$a_2^{(l)} = \frac{1}{3}\left(c_p^{(l)} + 2\sqrt{2} c_s^{(l)}\right), \tag{19}$$

where σ_m is the mean stress (an invariant of the stress tensor), s_{ij} are the components of the deviatoric stress tensor, and $c_s^{(l)} = \sqrt{G^{(l)}/\rho^{(l)}}$ and $c_p^{(l)} = \sqrt{(\lambda^{(l)} + 2\, G^{(l)})/\rho^{(l)}}$ are the shear- and dilatational-wave speeds, respectively, on either side of the fault. Using the symmetrized equations simplifies the analysis, but the developed methods may be implemented with the original variable set. The form of the symmetrized equations is not unique, and this symmetrization has been chosen since it results in the

physical energy [Slaughter, 2002] when the norm is defined as

$$\begin{aligned}\|\boldsymbol{q}(\cdot,t)\|^2 &= \int_{-\infty}^{0} \left(\boldsymbol{q}^{(2)}\right)^T \boldsymbol{q}^{(2)}\, dy + \int_{0}^{\infty} \left(\boldsymbol{q}^{(1)}\right)^T \boldsymbol{q}^{(1)}\, dy \\ &= \int_{-\infty}^{\infty} \left[\frac{\rho^{(l)}}{2} v_i v_i + \frac{1}{4G^{(l)}}\sigma_{ij}\left(\sigma_{ij} - \frac{\lambda^{(l)}}{3\lambda^{(l)}+2G^{(l)}}\sigma_{kk}\delta_{ij}\right)\right] dy,\end{aligned} \tag{20}$$

where the first term is the material kinetic energy, the second term is the elastic strain energy, and (l) is taken to be the proper value depending on the sign of the integration argument y. Note that (20) is a positive quantity by construction.

In order to fully specify the problem we need interface conditions relating the particle velocities and tractions on either side of the fault. The number of such interface conditions, which we will generically call boundary conditions, can be determined by considering the problem in characteristic form; the number of boundary conditions must equal to the number of waves propagating out of the fault [Kreiss, 1970]. For full tensor elasticity there are nine characteristic variables: three propagating to the right ($\boldsymbol{w}^{+(l)}$), three propagating to the left ($\boldsymbol{w}^{-(l)}$), and three stationary ($\boldsymbol{w}^{(l)}$). The three propagating waves moving in each direction correspond to the previously mentioned shear and dilatational waves. The characteristic variables are

$$\boldsymbol{w}^{\pm(l)} = \begin{bmatrix} w_{yx}^{\pm(l)} \\ w_{yy}^{\pm(l)} \\ w_{yz}^{\pm(l)} \end{bmatrix} = \begin{bmatrix} \sigma_{yx}^{(l)} \mp Z_s^{(l)} v_x^{(l)} \\ \sigma_{yy}^{(l)} \mp Z_p^{(l)} v_y^{(l)} \\ \sigma_{yz}^{(l)} \mp Z_s^{(l)} v_z^{(l)} \end{bmatrix}, \text{ with speeds } \begin{bmatrix} \pm c_s^{(l)} \\ \pm c_p^{(l)} \\ \pm c_s^{(l)} \end{bmatrix}, \tag{21}$$

$$\boldsymbol{w}^{(l)} = \begin{bmatrix} w_{xx}^{(l)} \\ w_{zz}^{(l)} \\ w_{xz}^{(l)} \end{bmatrix} = \begin{bmatrix} \sigma_{xx}^{(l)} - \frac{\lambda^{(l)}}{2\,G^{(l)}+\lambda^{(l)}}\sigma_{yy}^{(l)} \\ \sigma_{zz}^{(l)} - \frac{\lambda^{(l)}}{2\,G^{(l)}+\lambda^{(l)}}\sigma_{yy}^{(l)} \\ \sigma_{xz}^{(l)} \end{bmatrix}, \text{ all with speed 0,} \tag{22}$$

where superscript $\pm$ refers to direction of propagation, $Z_s^{(l)} = \rho^{(l)} c_s^{(l)}$ is the shear impedance, and $Z_p^{(l)} = \rho^{(l)} c_p^{(l)}$ the dilatational impedance.

From this it is clear that we need six boundary conditions relating the waves propagating out of the fault ($\boldsymbol{w}^{+(1)}$ and $\boldsymbol{w}^{-(2)}$) to the waves propagating into the fault ($\boldsymbol{w}^{-(1)}$ and $\boldsymbol{w}^{+(2)}$) and the stationary waves ($\boldsymbol{w}^{(1)}$ and $\boldsymbol{w}^{(2)}$):

$$\boldsymbol{w}^{+(1)}(0,t) = \boldsymbol{\mathcal{W}}^{+(1)}\left(\boldsymbol{w}^{-(1)}(0,t), \boldsymbol{w}^{+(2)}(0,t), \boldsymbol{w}^{(1)}(0,t), \boldsymbol{w}^{(2)}(0,t)\right), \tag{23}$$

$$\boldsymbol{w}^{-(2)}(0,t) = \boldsymbol{\mathcal{W}}^{-(2)}\left(\boldsymbol{w}^{-(1)}(0,t), \boldsymbol{w}^{+(2)}(0,t), \boldsymbol{w}^{(1)}(0,t), \boldsymbol{w}^{(2)}(0,t)\right). \tag{24}$$

With this notation, the problem in characteristic form is

$$\frac{\partial \boldsymbol{W}^{(l)}}{\partial t} = \boldsymbol{\Lambda}^{(l)} \frac{\partial \boldsymbol{W}^{(l)}}{\partial y}, \quad \boldsymbol{W}^{(l)} = \begin{bmatrix} \boldsymbol{w}^{+(l)} \\ \boldsymbol{w}^{-(l)} \\ \boldsymbol{w}^{(l)} \end{bmatrix}, \tag{25}$$

$$\boldsymbol{\Lambda}^{(l)} = \mathbf{diag}\begin{bmatrix} -c_s^{(l)} & -c_p^{(l)} & -c_s^{(l)} & c_s^{(l)} & c_p^{(l)} & c_s^{(l)} & 0 & 0 & 0 \end{bmatrix}, \tag{26}$$

with initial conditions

$$\boldsymbol{W}^{(1)}(y,0) = \widetilde{\boldsymbol{W}}^{(1)}(y), \quad \left(\widetilde{\boldsymbol{W}}^{(1)}(y) \equiv 0 \text{ if } y < 0\right), \tag{27}$$

$$\boldsymbol{W}^{(2)}(y,0) = \widetilde{\boldsymbol{W}}^{(2)}(y), \quad \left(\widetilde{\boldsymbol{W}}^{(2)}(y) \equiv 0 \text{ if } y > 0\right), \tag{28}$$

$$\widetilde{\boldsymbol{W}}^{(l)}(y) = \begin{bmatrix} \widetilde{\boldsymbol{w}}^{+(l)}(y) \\ \widetilde{\boldsymbol{w}}^{-(l)}(y) \\ \widetilde{\boldsymbol{w}}^{(l)}(y) \end{bmatrix}, \ \widetilde{\boldsymbol{w}}^{\pm(l)}(y) = \begin{bmatrix} \widetilde{w}_{yx}^{\pm(l)}(y) \\ \widetilde{w}_{yy}^{\pm(l)}(y) \\ \widetilde{w}_{yz}^{\pm(l)}(y) \end{bmatrix}, \ \widetilde{\boldsymbol{w}}^{(l)}(y) = \begin{bmatrix} \widetilde{w}_{xx}^{(l)}(y) \\ \widetilde{w}_{zz}^{(l)}(y) \\ \widetilde{w}_{xz}^{(l)}(y) \end{bmatrix}, \tag{29}$$

and boundary conditions (23) and (24). The exact solution can be found using the method of characteristics. To simplify the expressions we define the boundary conditions evaluated at a specific time as

$$\mathfrak{W}^{+(1)}(t) \equiv \boldsymbol{\mathcal{W}}^{+(1)}\left(\boldsymbol{w}^{-(1)}(0,t), \boldsymbol{w}^{+(2)}(0,t), \boldsymbol{w}^{(1)}(0), \boldsymbol{w}^{(2)}(0)\right), \tag{30}$$

$$\mathfrak{W}^{-(2)}(t) \equiv \boldsymbol{\mathcal{W}}^{-(2)}\left(\boldsymbol{w}^{-(1)}(0,t), \boldsymbol{w}^{+(2)}(0,t), \boldsymbol{w}^{(1)}(0), \boldsymbol{w}^{(2)}(0)\right), \tag{31}$$

so the exact solution for $y \geq 0$ is

$$\boldsymbol{w}^{+(1)}(y,t) = \begin{bmatrix} \widetilde{w}_{yx}^{+(1)}\left(y - c_s^{(1)}t\right) + \mathfrak{W}_{yx}^{+(1)}\left(y - c_s^{(1)}t\right) \\ \widetilde{w}_{yy}^{+(1)}\left(y - c_p^{(1)}t\right) + \mathfrak{W}_{yy}^{+(1)}\left(y - c_p^{(1)}t\right) \\ \widetilde{w}_{yz}^{+(1)}\left(y - c_s^{(1)}t\right) + \mathfrak{W}_{yz}^{+(1)}\left(y - c_s^{(1)}t\right) \end{bmatrix}, \tag{32}$$

$$\boldsymbol{w}^{-(1)}(y,t) = \begin{bmatrix} \widetilde{w}_{yx}^{-(1)}\left(y + c_s^{(1)}t\right) \\ \widetilde{w}_{yy}^{-(1)}\left(y + c_p^{(1)}t\right) \\ \widetilde{w}_{yz}^{-(1)}\left(y + c_s^{(1)}t\right) \end{bmatrix} \tag{33}$$

$$\boldsymbol{w}^{(1)}(y,t) = \widetilde{\boldsymbol{w}}^{(1)}(y), \tag{34}$$

and for $y \leq 0$ is

$$\boldsymbol{w}^{+(2)}(y,t) = \begin{bmatrix} \widetilde{w}_{yx}^{+(2)}\left(y - c_s^{(2)}t\right) \\ \widetilde{w}_{yy}^{+(2)}\left(y - c_p^{(2)}t\right) \\ \widetilde{w}_{yz}^{+(2)}\left(y - c_s^{(2)}t\right) \end{bmatrix} \tag{35}$$

$$\boldsymbol{w}^{-(2)}(y,t) = \begin{bmatrix} \widetilde{w}_{yx}^{-(2)}\left(y + c_s^{(2)}t\right) + \mathfrak{W}_{yx}^{-(2)}\left(y + c_s^{(2)}t\right) \\ \widetilde{w}_{yy}^{-(2)}\left(y + c_p^{(2)}t\right) + \mathfrak{W}_{yy}^{-(2)}\left(y + c_p^{(2)}t\right) \\ \widetilde{w}_{yz}^{-(2)}\left(y + c_s^{(2)}t\right) + \mathfrak{W}_{yz}^{-(2)}\left(y + c_s^{(2)}t\right) \end{bmatrix}, \tag{36}$$

$$\boldsymbol{w}^{(2)}(y,t) = \widetilde{\boldsymbol{w}}^{(2)}(y). \tag{37}$$

For the problem to be well-posed [Gustafsson et al., 1996] we also need the solution to be unique and to satisfy an energy estimate of the form

$$\|\boldsymbol{q}(\cdot,t)\| \leq K_c e^{\alpha_c t}\|\boldsymbol{q}(\cdot,0)\|, \tag{38}$$

where K_c and α_c are constants independent of the solution. In order to show that (38) holds it is sufficient to show that the boundary conditions lead to energy dissipation,

$$\frac{d\|q\|^2}{dt} \leq 0; \tag{39}$$

then by integration (38) holds with $\alpha_c = 0$ and $K_c = 1$.

For problems in elastodynamics the boundary conditions are generally not specified in characteristic form, but as nonlinear functions relating the particle velocities and stresses. Thus, we need to show that the boundary conditions in terms of the physical variables, outlined below, lead to energy dissipation and a unique solution.

To specify the boundary conditions in terms of the physical variables the definition of a jump function is needed:

$$[[g]] = g(0^+,t) - g(0^-,t) = \lim_{\varepsilon \to 0}\left(g(0+\varepsilon,t) - g(0-\varepsilon,t)\right). \tag{40}$$

Across the fault interface the particle velocity can be discontinuous, and we define the two components of slip velocity as

$$\boldsymbol{V}(t) = \begin{bmatrix} V_x(t) \\ V_z(t) \end{bmatrix} = \begin{bmatrix} [[v_x]] \\ [[v_z]] \end{bmatrix}, \quad V = \sqrt{\boldsymbol{V}^T\boldsymbol{V}}, \tag{41}$$

note that $V \geq 0$ (slightly different than V in Part 1), and the opening velocity as $\omega(t) = [[v_y]]$. The fault traction (specifically, the force per unit area of material (1) on material (2)), $\boldsymbol{T} = [\sigma_{yx}, \sigma_{yy}, \sigma_{yz}]^T$, must be continuous across the fault to satisfy Newton's third law (or momentum balance across a stationary discontinuity surface) [Freund, 1998]:

$$[[\sigma_{yi}]] = 0, \ i = x, y, z, \tag{42}$$

The normal stress, taken to be positive in compression, is

$$\sigma_n(t) = -\sigma_{yy}(0, t), \tag{43}$$

and the shear traction is

$$\boldsymbol{\tau}(t) = \begin{bmatrix} \sigma_{yx}(0, t) \\ \sigma_{yz}(0, t) \end{bmatrix}. \tag{44}$$

In this work, we make the following constitutive assumptions. First, we assume that the fault always experiences a compressive stress ($\sigma_n > 0$) such that it remains closed ($\omega = 0$). We also assume that the shear traction is a function of the slip velocity and the normal stress:

$$\boldsymbol{\tau} = \boldsymbol{F}(\sigma_n, \boldsymbol{V}). \tag{45}$$

Assuming that the fields go to zero as $y \to \pm\infty$, the energy dissipation rate is calculated using integration by parts as

$$\begin{aligned} \frac{d\|\boldsymbol{q}(\cdot, t)\|^2}{dt} &= 2 \int_{-\infty}^{0} \boldsymbol{q}^T \boldsymbol{A}^{(1)} \frac{\partial}{\partial t} \boldsymbol{q} \, dy + 2 \int_{0}^{\infty} \boldsymbol{q}^T \boldsymbol{A}^{(2)} \frac{\partial}{\partial t} \boldsymbol{q} \, dy \\ &= -\boldsymbol{V}^T \boldsymbol{\tau} + \omega \sigma_n = -\boldsymbol{V}^T \boldsymbol{F}(\sigma_n, \boldsymbol{V}), \end{aligned} \tag{46}$$

so the problem dissipates energy if $\boldsymbol{V}^T \boldsymbol{F}(\sigma_n, \boldsymbol{V}) \geq 0$; the expression $\boldsymbol{V}^T \boldsymbol{\tau}$ corresponds to the rate of energy dissipation per unit fault area due to frictional work on the fault.

In order for the problem to be well-posed a unique solution must exists. Existence can be proven with the method of characteristics and uniqueness with the energy method. For linear problems with linear boundary conditions uniqueness follows directly from the energy dissipation estimate, but as noted in Part 1 this is not the case for problems with nonlinear boundary conditions. As in Part 1, further restrictions are necessary on the friction law $\boldsymbol{F}$ for existence and uniqueness.

Existence via the Method of Characteristics

In order to show that a solution exsists we derive conditions on the friction law such that it implicitly represents unique characteristic boundary conditions of the form (23) and (24). There is, in general, no closed form expression for $\boldsymbol{\mathcal{W}}^{+(1)}$ and $\boldsymbol{\mathcal{W}}^{-(2)}$ for arbitrary $\boldsymbol{F}(\sigma_n, \boldsymbol{V})$ and the implicit function theorem is needed to show that such functions exist; see App. A for the bracketed Newton's method we use for finding these functions in practice.

Since we do not allow for fault opening ($\omega = 0$), a closed form expression can be determined for $\mathcal{W}_{yy}^{+(1)}$ and $\mathcal{W}_{yy}^{-(2)}$. Noting that

$$\begin{aligned}
\sigma_n(t) =& -\sigma_{yy}(0^{\pm}, t) \\
=& -\frac{1}{2}[w_{yy}^{-(l)}(0,t) + w_{yy}^{+(l)}(0,t)],\ l = 1, 2, \qquad (47) \\
\omega(t) =& [[v_y]], \\
=& \frac{1}{2\ Z_p^{(1)}}\left[w_{yy}^{-(1)}(0,t) - w_{yy}^{+(1)}(0,t)\right] \qquad (48) \\
& - \frac{1}{2\ Z_p^{(2)}}\left[w_{yy}^{-(2)}(0,t) - w_{yy}^{+(2)}(0,t)\right],
\end{aligned}$$

we solve for $\mathcal{W}_{yy}^{+(1)} = w_{yy}^{+(1)}(0,t)$ and $\mathcal{W}_{yy}^{-(2)} = w_{yy}^{-(2)}(0,t)$ using $\omega = 0$ and continuity of σ_n across the fault:

$$\begin{bmatrix} \mathcal{W}_{yy}^{+(1)} \\ \mathcal{W}_{yy}^{-(2)} \end{bmatrix} = \frac{1}{Z_p^{(1)} + Z_p^{(2)}} \begin{bmatrix} Z_p^{(2)} - Z_p^{(1)} & 2Z_p^{(1)} \\ 2Z_p^{(2)} & Z_p^{(1)} - Z_p^{(2)} \end{bmatrix} \begin{bmatrix} w_{yy}^{-(1)} \\ w_{yy}^{+(2)} \end{bmatrix}. \qquad (49)$$

In order to find conditions on the friction law $\boldsymbol{F}(\sigma_n, \boldsymbol{V})$ such that $\mathcal{W}_{yx}^{+(1)}$, $\mathcal{W}_{yz}^{+(1)}$, $\mathcal{W}_{yx}^{-(2)}$, and $\mathcal{W}_{yz}^{-(2)}$ are single-valued functions, the implicit function theorem is needed (in what follows we assume that $\boldsymbol{F}(\sigma_n, \boldsymbol{V})$ is smooth). Namely, we can write the boundary conditions as

$$0 = \begin{bmatrix} [[\sigma_{yx}]] \\ [[\sigma_{yz}]] \\ \begin{bmatrix} \sigma_{yx}(0^+, t) \\ \sigma_{yz}(0^+, t) \end{bmatrix} - \boldsymbol{F}\left(\sigma_n(t), \begin{bmatrix} [[v_x]] \\ [[v_z]] \end{bmatrix}\right) \end{bmatrix}, \qquad (50)$$

where the first two lines are due to continuity of stress (42) and the second two lines are due the friction law (45). Then, using the characteristic

variables (21), this can be rewritten as a function

$$\begin{aligned}0 =& \frac{1}{2}\begin{bmatrix} w_{yx}^{-(1)} + \mathcal{W}_{yx}^{+(1)} - \mathcal{W}_{yx}^{-(2)} - w_{yx}^{+(2)} \\ w_{yz}^{-(1)} + \mathcal{W}_{yz}^{+(1)} - \mathcal{W}_{yz}^{-(2)} - w_{yz}^{+(2)} \\ \begin{bmatrix} w_{yx}^{-(1)} + \mathcal{W}_{yx}^{+(1)} \\ w_{yz}^{-(1)} + \mathcal{W}_{yz}^{+(1)} \end{bmatrix} - 2\boldsymbol{F}\left(\sigma_n, \boldsymbol{V}(t)\right) \end{bmatrix} \\ =& \boldsymbol{g}(w_{yx}^{-(1)}, w_{yz}^{-(1)}, w_{yx}^{+(2)}, w_{yz}^{+(2)}), \end{aligned} \tag{51}$$

$$\boldsymbol{V} = \begin{bmatrix} V_x \\ V_z \end{bmatrix} = \frac{1}{2Z_s^{(1)}} \begin{bmatrix} w_{yx}^{-(1)} - \mathcal{W}_{yx}^{+(1)} \\ w_{yz}^{-(1)} - \mathcal{W}_{yz}^{+(1)} \end{bmatrix} - \frac{1}{2Z_s^{(2)}} \begin{bmatrix} \mathcal{W}_{yx}^{-(2)} - w_{yx}^{+(2)} \\ \mathcal{W}_{yz}^{-(2)} - w_{yz}^{+(2)} \end{bmatrix}, \tag{52}$$

and unique functions $\mathcal{W}_{yx}^{+(1)}$, $\mathcal{W}_{yz}^{+(1)}$, $\mathcal{W}_{yx}^{-(2)}$, and $\mathcal{W}_{yz}^{-(2)}$ exist if the Jacobian of $\boldsymbol{g}$ is nonsingular for all inputs,

$$\begin{aligned} 0 \neq& \det\left(\begin{bmatrix} \frac{\partial \boldsymbol{g}}{\partial \mathcal{W}_{yx}^{-(1)}} & \frac{\partial \boldsymbol{g}}{\partial \mathcal{W}_{yz}^{-(1)}} & \frac{\partial \boldsymbol{g}}{\partial \mathcal{W}_{yx}^{+(2)}} & \frac{\partial \boldsymbol{g}}{\partial \mathcal{W}_{yz}^{+(2)}} \end{bmatrix}\right) \\ =& \frac{1}{2}\det\left(\begin{bmatrix} 1 & 0 & -1 & 0 \\ 0 & 1 & 0 & -1 \\ 1 & 0 & 0 & 0 \\ 0 & 1 & 0 & 0 \end{bmatrix} + \begin{bmatrix} 0 & 0 & 0 & 0 \\ 0 & 0 & 0 & 0 \\ \frac{2}{Z_s^{(1)}}\frac{\partial \boldsymbol{F}}{\partial V_x} & \frac{2}{Z_s^{(1)}}\frac{\partial \boldsymbol{F}}{\partial V_z} & \frac{2}{Z_s^{(2)}}\frac{\partial \boldsymbol{F}}{\partial V_x} & \frac{2}{Z_s^{(2)}}\frac{\partial \boldsymbol{F}}{\partial V_z} \end{bmatrix}\right) \\ =& \frac{1}{2}\det\left(\begin{bmatrix} 1 & 0 \\ 0 & 1 \end{bmatrix} + \left(\frac{2}{Z_s^{(1)}} + \frac{2}{Z_s^{(2)}}\right)\boldsymbol{J_F}\right), \end{aligned} \tag{53}$$

$$\boldsymbol{J_F} = \begin{bmatrix} \frac{\partial \boldsymbol{F}}{\partial V_x} & \frac{\partial \boldsymbol{F}}{\partial V_z} \end{bmatrix}, \tag{54}$$

where $\partial \boldsymbol{F}/\partial V_i$ is a 2-vector and $\boldsymbol{J_F}$ is the Jacobian of $\boldsymbol{F}$ with respect to $\boldsymbol{V}$. For any proposed friction law $\boldsymbol{F}(\sigma_n, \boldsymbol{V})$ these conditions need to be verified.

It is commonly assumed in frictional sliding models that $\boldsymbol{F}$ and $\boldsymbol{V}$ are in the same direction and that $\boldsymbol{F}$ is proportional to σ_n,

$$\boldsymbol{F}(\sigma_n, \boldsymbol{V}) = \sigma_n \frac{f(V)}{V}\boldsymbol{V}, \quad f(V) \geq 0 \text{ for all } V \geq 0, \tag{55}$$

where the friction coefficient $f(V)$ captures the instantaneous, not steady state, velocity dependence. Under this assumption, $\boldsymbol{J_F}$ is

$$\boldsymbol{J_F} = \sigma_n \left\{ \frac{f'(V)V - f(V)}{V^3} \begin{bmatrix} V_x^2 & V_x V_z \\ V_x V_z & V_z^2 \end{bmatrix} + \frac{f(V)}{V} \begin{bmatrix} 1 & 0 \\ 0 & 1 \end{bmatrix} \right\}, \tag{56}$$

and the determinant condition (53) becomes

$$0 \neq \frac{1}{2V}\left[V + \frac{\sigma_n}{\tilde{Z}_s}\, f(V)\right]\left[1 + \frac{\sigma_n}{\tilde{Z}_s}\, f'(V)\right], \quad \tilde{Z}_s = \frac{2\, Z_s^{(1)}\, Z_s^{(2)}}{Z_s^{(1)} + Z_s^{(2)}}. \tag{57}$$

Thus, the condition for uniqueness is $f'(V) \neq -\tilde{Z}_s/\sigma_n$. Since $f(V) \geq 0$ for all V this implies that $f'(V) > -\tilde{Z}_s/\sigma_n$ (if $f'(V) < -\tilde{Z}_s/\sigma_n$ for all V then the condition $f(V) \geq 0$ would be violated for sufficiently large V).

The friction laws used in this work, and those supported by experiments, are instantaneously velocity strengthening, that is, $f'(V) \geq 0$ for all V; hence, the conditions of the implicit function theorem are satisfied. Since the implicit function theorem guarantees unique characteristic boundary conditions if (57) hold, we can compute a solution using the method of characteristics, which implies existence.

Uniqueness via the Energy Method

Assume that we have two solutions $\boldsymbol{q}_1$ and $\boldsymbol{q}_2$ with the same initial data $\boldsymbol{q}_1(y,0) = \boldsymbol{q}_2(y,0)$. The difference of these two solutions $\Delta\boldsymbol{q} = \boldsymbol{q}_1 - \boldsymbol{q}_2$ satisfies the governing equations (13) with initial data $\Delta\boldsymbol{q}(y,0) = \boldsymbol{0}$ and boundary conditions

$$0 = \left[\left[(\sigma_{yy})_1\right]\right] = \left[\left[(\sigma_{yy})_2\right]\right], \tag{58}$$

$$0 = \omega_1(t) = \omega_2(t), \tag{59}$$

$$\Delta\boldsymbol{\tau} = \boldsymbol{F}\left((\sigma_n)_1, \boldsymbol{V}_1\right) - \boldsymbol{F}\left((\sigma_n)_2, \boldsymbol{V}_2\right). \tag{60}$$

If we can show that the energy dissipation rate for solution difference,

$$\frac{d\|\Delta\boldsymbol{q}(\cdot,t)\|}{dt} = -\Delta\omega\Delta\sigma_n - \Delta\boldsymbol{V}^T\Delta\boldsymbol{\tau} = -\Delta\boldsymbol{V}^T\Delta\boldsymbol{\tau}, \tag{61}$$

is negative semidefinite then uniqueness follows.

Since σ_{yy}, v_y, σ_{xx}, and σ_{zz} are decoupled from the rest of the variables, in the sense that they are not affected by the other variables in the governing equations and boundary conditions, they can be considered independently. Defining $\boldsymbol{\theta}^{(l)}$ to be the portion of $\boldsymbol{q}$ associated with these variables, i.e.,

$$\boldsymbol{\theta}^{(l)} = \frac{1}{\sqrt{2\rho^{(l)}}}\begin{bmatrix} \rho^{(l)}\, v_y \\ \sqrt{2}s_{xx}/(2c_s^{(l)}) + \sigma_m/c_p^{(l)} \\ \sqrt{2}s_{yy}/(2c_s^{(l)}) + \sigma_m/c_p^{(l)} \\ \sqrt{2}s_{zz}/(2c_s^{(l)}) + \sigma_m/c_p^{(l)} \end{bmatrix} \tag{62}$$

see (14), the energy estimate for the difference is

$$\frac{d}{dt}\|\Delta\boldsymbol{\theta}\|_2^2 = -\Delta\omega\ \Delta\sigma_n = 0, \tag{63}$$

and thus uniqueness of these variables follows, i.e., $\boldsymbol{\theta}_1(y,t) = \boldsymbol{\theta}_2(y,t)$.

Now to prove uniqueness of the remaining variables we need to use the following identity

$$\begin{aligned}\Delta\boldsymbol{\tau} =& \boldsymbol{F}\left(\sigma_n, \boldsymbol{V}_1\right) - \boldsymbol{F}\left(\sigma_n, \boldsymbol{V}_2\right) \\ =& \int_0^1 \left(\frac{\partial \boldsymbol{F}}{\partial V_x}\left(\boldsymbol{V}_2 + s\Delta\boldsymbol{V}\right)\Delta V_x + \frac{\partial \boldsymbol{F}}{\partial V_z}\left(\boldsymbol{V}_2 + s\Delta\boldsymbol{V}\right)\Delta V_z \right) ds \\ =& \int_0^1 \boldsymbol{J}_{\boldsymbol{F}}\left(\boldsymbol{V}_2 + s\Delta\boldsymbol{V}\right)\Delta\boldsymbol{V}\, ds,\end{aligned} \tag{64}$$

where $\boldsymbol{J}_{\boldsymbol{F}}(\boldsymbol{V})$ is the Jacobian of $\boldsymbol{F}$ with respect to $\boldsymbol{V}$ as defined in (54). Note since σ_{yy} is unique, as shown above, we have let $\sigma_n = (\sigma_n)_1 = (\sigma_n)_2$ in (64). Using (64) in (61) it follows that if $\boldsymbol{J}_{\boldsymbol{F}}(\boldsymbol{V})$ is positive semidefinite then (61) is negative semidefinite.

Assuming that $\boldsymbol{F}$ is of form (55) then $\boldsymbol{J}_{\boldsymbol{F}}$ is symmetric, see (56), with eigenvalues $f(V)/V$ and $f'(V)$, i.e., $\boldsymbol{J}_F$ is positive semidefinite if $f(V) \geq 0$ and $f'(V) \geq 0$ as is the case for all physical friction laws. Thus we have shown that sufficient conditions for well-posedness are a friction law of the form (55) with $f'(V) \geq 0$.

Mathematically the problem is likely well-posed with weaker conditions on the friction law, as was the case in Part 1, but here we have limited ourselves to those friction laws supported by experimental evidence.

2.1. Rate-and-State Friction

For the friction laws used in many earthquake problems, the friction coefficient depends not only on the current slip velocity but the history of sliding as well. This is captured through the use of a state variable ψ which evolves in time according to a differential evolution equation; this is known as rate-and-state friction [Dieterich, 1979, Ruina, 1983, Rice, 1983]. In this work, the following form of rate-and-state friction is used [Lapusta et al., 2000, Noda et al., 2009]:

$$f(V,\psi) = a \operatorname{arcsinh}\left(\frac{V}{2V_0}\exp\left(\frac{\psi}{a}\right)\right), \tag{65}$$

$$\frac{d\psi}{dt} = -\frac{V}{L}\left[f(V,\psi) - f_{ss}(V)\right], \tag{66}$$

where L is the state evolution distance, a is the direct effect parameter (see Figure 1(a)) and V_0 is an arbitrary reference velocity. This model describes a fault that is instantaneously velocity-strengthening ($\partial f/\partial V > 0$) and evolution of $f(V,\psi)$ toward $f_{ss}(V)$ over a characteristic slip distance L.

The steady state friction coefficient, $f_{ss}(V)$, is modeled in a variety of ways in the literature; we use a model that has mild velocity dependence at low velocities and more extreme weakening at high velocities (see Figure 1(b)):

$$f_{ss}(V) = f_w + [f_{LV}(V) - f_w] \left[1 + \left(\frac{V}{V_w}\right)^n\right]^{-1/n}, \tag{67}$$

$$f_{LV}(V) = f_0 - (b-a) \ln\left(\frac{V}{V_0}\right), \tag{68}$$

where we use $n = 8$, f_0 is the steady state friction coefficients at V_0, f_w is the steady state friction coefficient at high velocities, V_w is the weakening velocity, and b is the evolution effect parameter; a and V_0 are the same as in (65) [Noda et al., 2009]. The onset of extreme velocity-weakening behavior for $V > V_w$ is commonly observed in high velocity friction experiments [Tsutsumi and Shimamoto, 1997, Hirose and Shimamoto, 2005, Beeler et al., 2008, Rice, 2006].

3. Discrete Solution: SAT Method

Governing equations (13) can be discretized using SBP operators as

$$\frac{d\boldsymbol{q}^{(l)}}{dt} = \left(\boldsymbol{H}^{-1}\boldsymbol{Q} \otimes \boldsymbol{A}^{(l)}\right) \boldsymbol{q}^{(l)}, \tag{69}$$

$$\boldsymbol{q}^{(1)} = \left[\left(\boldsymbol{q}_0^{(1)}\right)^T \left(\boldsymbol{q}_1^{(1)}\right)^T \cdots\right]^T, \; \boldsymbol{q}^{(2)} = \left[\cdots \left(\boldsymbol{q}_{-1}^{(2)}\right)^T \left(\boldsymbol{q}_0^{(2)}\right)^T\right]^T, \tag{70}$$

$$\|\boldsymbol{q}^{(l)}(t)\|_h^2 = \left(\boldsymbol{q}^{(l)}\right)^T (\boldsymbol{H} \otimes \boldsymbol{I}_9) \left(\boldsymbol{q}^{(l)}\right), \tag{71}$$

$$\|\boldsymbol{q}(t)\|_h^2 = \|\boldsymbol{q}^{(1)}(t)\|_h^2 + \|\boldsymbol{q}^{(2)}(t)\|_h^2, \;\; \boldsymbol{q} = \left[\left(\boldsymbol{q}^{(2)}\right)^T \left(\boldsymbol{q}^{(1)}\right)^T\right]^T, \tag{72}$$

where $\boldsymbol{q}_0^{(1)}$ and $\boldsymbol{q}_0^{(2)}$ are collocated variables on the two sides of the fault (see Figure 2) and $\otimes$ is the Kronecker product of two matrices defined as

$$\boldsymbol{A} \otimes \boldsymbol{B} = \begin{bmatrix} A_{00}\boldsymbol{B} & \cdots & A_{0N}\boldsymbol{B} \\ \vdots & \ddots & \vdots \\ A_{N0}\boldsymbol{B} & \cdots & A_{NN}\boldsymbol{B} \end{bmatrix}. \tag{73}$$

The energy of the discrete solution is defined in an analogous manner to that in the continuous problem (20) as

$$\|\boldsymbol{q}(t)\|_h^2 = \left(\boldsymbol{q}^{(1)}\right)^T (\boldsymbol{H} \otimes \boldsymbol{I}_9)\, \boldsymbol{q}^{(1)} + \left(\boldsymbol{q}^{(2)}\right)^T (\boldsymbol{H} \otimes \boldsymbol{I}_9)\, \boldsymbol{q}^{(2)}. \tag{74}$$

To enforce the boundary conditions we use the SAT method in characteristic form. By characteristic form we mean that the boundary conditions formulated in terms of (23) and (24) are used, and not the boundary conditions formulated in terms of the physical variables (45). This is because, as shown in Part 1, using the physical variables results in an arbitrarily stiff system of ODEs which would necessitate the use of implicit methods for efficient time integration. The characteristic SAT method for these equations is

$$\frac{d\boldsymbol{q}^{(l)}}{dt} = \left(\boldsymbol{H}^{-1}\boldsymbol{Q} \otimes \boldsymbol{A}^{(l)}\right) \boldsymbol{q}^{(l)} + \boldsymbol{H}^{-1}\boldsymbol{e}_0^{(l)} \otimes \boldsymbol{\Sigma}\boldsymbol{B}_0^{(l)}, \tag{75}$$

$$\boldsymbol{B}_0^{(1)} = \begin{bmatrix} 1 \\ 0 \\ 0 \end{bmatrix} \otimes \left[\boldsymbol{w}_0^{+(1)} - \boldsymbol{\mathcal{W}}^{+(1)}\left(\boldsymbol{w}_0^{-(1)}, \boldsymbol{w}_0^{+(2)}, \boldsymbol{w}_0^{(1)}, \boldsymbol{w}_0^{(2)}\right)\right], \tag{76}$$

$$\boldsymbol{B}_0^{(2)} = \begin{bmatrix} 1 \\ 0 \\ 0 \end{bmatrix} \otimes \left[\boldsymbol{w}_0^{-(2)} - \boldsymbol{\mathcal{W}}^{-(2)}\left(\boldsymbol{w}_0^{-(1)}, \boldsymbol{w}_0^{+(2)}, \boldsymbol{w}_0^{(1)}, \boldsymbol{w}_0^{(2)}\right)\right], \tag{77}$$

$$\boldsymbol{e}_0^{(1)} = \begin{bmatrix} 1 & 0 & 0 & \cdots \end{bmatrix}^T, \; \boldsymbol{e}_0^{(2)} = \begin{bmatrix} \cdots & 0 & 0 & 1 \end{bmatrix}^T, \tag{78}$$

where the discrete characteristic variables are analogous to those defined in (21) and (22).

The energy dissipation rate is

$$\frac{d\|\boldsymbol{q}\|_h^2}{dt} = v_i^{(2)}\sigma_{yi}^{(2)} - v_i^{(1)}\sigma_{yi}^{(1)} + 2\left(\boldsymbol{q}_0^{(1)}\right)^T \boldsymbol{\Sigma}^{(1)}\boldsymbol{B}_0^{(1)} + 2\left(\boldsymbol{q}_0^{(2)}\right)^T \boldsymbol{\Sigma}^{(2)}\boldsymbol{B}_0^{(2)}, \tag{79}$$

where we have utilized the SBP property (10) of the difference operator, assumed that $\boldsymbol{\Sigma}^{(l)}$ is symmetric, and here (as in subsequent expression for the energy dissipation) the grid data is the boundary data $\boldsymbol{q}_0^{(l)}$, i.e., $v_i^{(l)} = \left(v_i^{(l)}\right)_0$ and $\sigma_{ij}^{(l)} = \left(\sigma_{ij}^{(l)}\right)_0$. We now make the assumption that the penalty matrices $\boldsymbol{\Sigma}^{(l)}$ can be chosen so that

$$2\left(\boldsymbol{q}_0^{(1)}\right)^T \boldsymbol{\Sigma}^{(1)}\boldsymbol{B}_0^{(1)} = -\left(\boldsymbol{w}_0^{+(1)}\right)^T \mathbf{diag}\begin{bmatrix} \frac{1}{2Z_s^{(1)}} \\ \frac{1}{2Z_p^{(1)}} \\ \frac{1}{2Z_s^{(1)}} \end{bmatrix} \left(\boldsymbol{w}_0^{+(1)} - \boldsymbol{\mathcal{W}}^{+(1)}\right), \tag{80}$$

$$2\left(\boldsymbol{q}_0^{(2)}\right)^T \boldsymbol{\Sigma}^{(2)}\boldsymbol{B}_0^{(2)} = -\left(\boldsymbol{w}_0^{-(2)}\right)^T \mathbf{diag}\begin{bmatrix} \frac{1}{2Z_s^{(2)}} \\ \frac{1}{2Z_p^{(2)}} \\ \frac{1}{2Z_s^{(2)}} \end{bmatrix} \left(\boldsymbol{w}_0^{-(2)} - \boldsymbol{\mathcal{W}}^{-(2)}\right), \tag{81}$$

where the boundary notation has been simplified to be

$$\boldsymbol{\mathcal{W}}^{+(1)} \equiv \boldsymbol{\mathcal{W}}^{+(1)}\left(\boldsymbol{w}_0^{-(1)}, \boldsymbol{w}_0^{+(2)}, \boldsymbol{w}_0^{(1)}, \boldsymbol{w}_0^{(2)}\right), \tag{82}$$

$$\boldsymbol{\mathcal{W}}^{-(2)} \equiv \boldsymbol{\mathcal{W}}^{-(2)}\left(\boldsymbol{w}_0^{-(1)}, \boldsymbol{w}_0^{+(2)}, \boldsymbol{w}_0^{(1)}, \boldsymbol{w}_0^{(2)}\right). \tag{83}$$

With this assumption the energy dissipation rate (79) becomes

$$\begin{aligned}\frac{d\|\boldsymbol{q}\|_h^2}{dt} = \sum_{i=x,y,z}\Bigg[&- \frac{1}{4\ Z_i^{(1)}}\left(w_{yi}^{-(1)} - \mathcal{W}_{yi}^{+(1)}\right)\left(w_{yi}^{-(1)} + \mathcal{W}_{yi}^{+(1)}\right) \\ &+ \frac{1}{4\ Z_i^{(2)}}\left(w_{yi}^{-(2)} - \mathcal{W}_{yi}^{+(2)}\right)\left(w_{yi}^{-(2)} + \mathcal{W}_{yi}^{+(2)}\right) \\ &- \frac{1}{4Z_i^{(1)}}\left(w_{yi}^{+(1)} - \mathcal{W}_{yi}^{+(1)}\right)^2 - \frac{1}{4Z_i^{(2)}}\left(w_{yi}^{-(2)} - \mathcal{W}_{yi}^{-(2)}\right)^2\Bigg],\end{aligned} \tag{84}$$

where the physical variables have been replaced with the characteristic variables using (21) and (22), and the impedances are defined as $Z_x^{(l)} = Z_z^{(l)} = Z_s^{(l)}$ and $Y_y^{(l)} = Z_p^{(l)}$. Since $\mathcal{W}_{yi}^{\pm(l)}$ implicitly represent boundary conditions formulated in terms of the physical variables, we can define

$$\hat{\sigma}_{yi} \equiv \frac{1}{2}\left(w_{yi}^{-(1)} + \mathcal{W}_{yi}^{+(1)}\right) = \frac{1}{2}\left(\mathcal{W}_{yi}^{+(2)} + w_{yi}^{-(2)}\right), \tag{85}$$

$$\hat{v}_i^{(1)} \equiv \frac{1}{2\ Z_i^{(1)}}\left(w_{yi}^{-(1)} - \mathcal{W}_{yi}^{+(1)}\right), \tag{86}$$

$$\hat{v}_i^{(2)} \equiv \frac{1}{2\ Z_i^{(2)}}\left(w_{yi}^{-(2)} - \mathcal{W}_{yi}^{+(2)}\right), \tag{87}$$

$$\hat{\omega} \equiv \hat{v}_y^{(1)} - \hat{v}_y^{(2)}, \qquad \hat{\sigma}_n \equiv -\hat{\sigma}_{yy}, \tag{88}$$

$$\hat{\boldsymbol{V}} \equiv \begin{bmatrix}\hat{v}_x^{(1)} - \hat{v}_x^{(2)} \\ \hat{v}_z^{(1)} - \hat{v}_z^{(2)}\end{bmatrix}, \qquad \hat{\boldsymbol{\tau}} \equiv \begin{bmatrix}\hat{\sigma}_{yx} \\ \hat{\sigma}_{yz}\end{bmatrix}, \tag{89}$$

which exactly satisfy the continuity conditions (42), the boundary condition (45), and $\hat{\omega} = 0$. With these definitions the energy dissipation rate (84) is

$$\begin{aligned}\frac{d\|\boldsymbol{q}\|_h^2}{dt} = &- \hat{\boldsymbol{V}}^T\hat{\boldsymbol{\tau}} \\ &- \sum_{i=x,y,z}\left[\frac{1}{4Z_i^{(1)}}\left(w_{yi}^{+(1)} - \mathcal{W}_{yi}^{+(1)}\right)^2 + \frac{1}{4Z_i^{(2)}}\left(w_{yi}^{-(2)} - \mathcal{W}_{yi}^{-(2)}\right)^2\right],\end{aligned} \tag{90}$$

where the term in brackets is a numerical damping term that goes to zero as the grid is refined. Thus, the scheme dissipates energy slightly faster than the continuous problem (46) and the method is strictly stable if symmetric penalty matrices can be found such that (80) and (81) hold. This can be done by choosing the penalty matrices:

$$\boldsymbol{\Sigma}^{(l)} = \begin{bmatrix} \Sigma_2^{(l)} & 0 & 0 & 0 & 0 & 0 & \Sigma_1^{(l)} & 0 & 0 \\ 0 & \Sigma_2^{(l)} & 0 & \Sigma_3^{(l)} & \Sigma_4^{(l)} & \Sigma_3^{(l)} & 0 & 0 & 0 \\ 0 & 0 & \Sigma_2^{(l)} & 0 & 0 & 0 & 0 & 0 & \Sigma_1^{(l)} \\ 0 & \Sigma_3^{(l)} & 0 & 0 & 0 & 0 & 0 & 0 & 0 \\ 0 & \Sigma_4^{(l)} & 0 & 0 & 0 & 0 & 0 & 0 & 0 \\ 0 & \Sigma_3^{(l)} & 0 & 0 & 0 & 0 & 0 & 0 & 0 \\ \Sigma_1^{(l)} & 0 & 0 & 0 & 0 & 0 & 0 & 0 & 0 \\ 0 & 0 & 0 & 0 & 0 & 0 & 0 & 0 & 0 \\ 0 & 0 & \Sigma_1^{(l)} & 0 & 0 & 0 & 0 & 0 & 0 \end{bmatrix}, \tag{91}$$

$$\Sigma_1^{(l)} = -\frac{1}{2\sqrt{2\rho^{(l)}}},\ \Sigma_2^{(1)} = -\Sigma_1^{(1)},\ \Sigma_2^{(2)} = \Sigma_1^{(2)}, \tag{92}$$

$$\Sigma_3^{(l)} = -\frac{1}{12\sqrt{\rho^{(l)}}}\left(\sqrt{2} - 2\frac{c_s^{(l)}}{c_p^{(l)}}\right),\ \Sigma_4^{(l)} = -\frac{1}{12\sqrt{\rho^{(l)}}}\left(\sqrt{2} + 4\frac{c_s^{(l)}}{c_p^{(l)}}\right). \tag{93}$$

The scheme can be written in terms of the original variables (11) and (12):

$$\frac{d\boldsymbol{v}_i^{(l)}}{dt} = \frac{1}{\rho^{(l)}}\ \boldsymbol{H}^{-1}\ \boldsymbol{Q}\ \boldsymbol{\sigma}_{yi} - c_s^{(l)}(v_i^{(l)} - \hat{v}_i^{(l)})\boldsymbol{H}^{-1}\boldsymbol{e}_0^{(l)},\ i = x, z, \tag{94}$$

$$\frac{d\boldsymbol{\sigma}_{yi}^{(l)}}{dt} = G^{(l)}\ \boldsymbol{H}^{-1}\ \boldsymbol{Q}\ \boldsymbol{v}_i - c_s^{(l)}(\sigma_{yi}^{(l)} - \hat{\sigma}_{yi})\boldsymbol{H}^{-1}\boldsymbol{e}_0^{(l)},\ i = x, z, \tag{95}$$

$$\frac{d\boldsymbol{\sigma}_{ii}^{(l)}}{dt} = \lambda^{(l)}\ \boldsymbol{H}^{-1}\ \boldsymbol{Q}\ \boldsymbol{v}_y - c_p^{(l)}(\sigma_{ii}^{(l)} - \hat{\sigma}_{ii})\boldsymbol{H}^{-1}\boldsymbol{e}_0^{(l)},\ i = x, z, \tag{96}$$

$$\frac{d\boldsymbol{v}_y^{(l)}}{dt} = \frac{1}{\rho^{(l)}}\ \boldsymbol{H}^{-1}\ \boldsymbol{Q}\ \boldsymbol{\sigma}_{yy} - c_p^{(l)}(v_y^{(l)} - \hat{v}_y^{(l)})\boldsymbol{H}^{-1}\boldsymbol{e}_0^{(l)}, \tag{97}$$

$$\frac{d\boldsymbol{\sigma}_{yy}^{(l)}}{dt} = (\lambda^{(l)} + 2\ G^{(l)})\ \boldsymbol{H}^{-1}\ \boldsymbol{Q}\ \boldsymbol{v}_y - c_p^{(l)}(\sigma_{yy}^{(l)} - \hat{\sigma}_{yy}^{(l)})\boldsymbol{H}^{-1}\boldsymbol{e}_0^{(l)}, \tag{98}$$

$$\frac{d\boldsymbol{\sigma}_{xz}^{(l)}}{dt} = 0, \tag{99}$$

where $\hat{v}_i^{(l)}$ and $\hat{\sigma}_{yi}$ are defined by (85)-(87), there is no summation over i in

(96), and

$$\hat{\sigma}_{xx}^{(l)} = w_{xx}^{(l)} + \frac{\lambda^{(l)}}{2\,G^{(l)} + \lambda^{(l)}}\hat{\sigma}_{yy}, \qquad \hat{\sigma}_{zz}^{(l)} = w_{zz}^{(l)} + \frac{\lambda^{(l)}}{2\,G^{(l)} + \lambda^{(l)}}\hat{\sigma}_{yy}; \tag{100}$$

see (21) and (22). The variables $\boldsymbol{v}_x^{(l)}$, $\boldsymbol{v}_z^{(l)}$, $\boldsymbol{\sigma}_{yx}^{(l)}$, and $\boldsymbol{\sigma}_{yz}^{(l)}$ have the penalty weight $c_s^{(l)}\ \boldsymbol{H}^{-1}$ and all the others have the penalty weight $c_p^{(l)}\ \boldsymbol{H}^{-1}$. The values $\hat{v}_i^{(l)}$ and $\hat{\sigma}_{yj}$, not the grid variables, are used to integrate the state evolution equation (66) for rate-and-state friction.

4. Computational Test

In order to test the method the physical parameters of Table 1 are used. The elastic properties have been chosen so there is a 10% contrast in wave speeds across the fault and no contrast in density. The initial conditions are

$$\begin{bmatrix} v_x(y,0) \\ \sigma_{yx}(y,0) \\ v_z(y,0) \\ \sigma_{yz}(y,0) \\ v_y(y,0) \\ \sigma_{yy}(y,0) \\ \sigma_{xx}(y,0) \\ \sigma_{zz}(y,0) \end{bmatrix} = \begin{bmatrix} \bar{v}_x \\ \bar{\sigma}_{yx} \\ \bar{v}_z \\ \bar{\sigma}_{yz} \\ \bar{v}_y \\ \bar{\sigma}_{yy} \\ \bar{\sigma}_{xx} \\ \bar{\sigma}_{zz} \end{bmatrix} + 100 \begin{bmatrix} g(y,10,3/2)/Z_s \\ g(y,10,3/2) \\ g(y,\ 8,\quad 1)/Z_s \\ g(y,\ 8,\quad 1) \\ g(y,13,\quad 2)/Z_p \\ g(y,13,\quad 2) \\ g(y,13,\quad 2) \\ g(y,13,\quad 2) \end{bmatrix}, \tag{101}$$

$$g(y,y_0,r_0) = \sin\left(\frac{\pi}{2}\,y\right)\ \exp\left(\frac{1}{2}\left(\frac{y-y_0}{r_0}\right)^2\right), \tag{102}$$

which correspond to three wave packets moving to the left (into the fault): two shear waves with polarizations in the x-direction (influencing σ_{yx} and v_x) and z-direction (influencing σ_{yz} and v_z), and one dilatational wave pulse (influencing σ_{yy} and v_y); see (21). The incident tensile (normal) stress is such that the fault remains closed; hence, the solution in the medium is smooth for all time, but the solution is discontinuous or non-smooth across the fault. For computations we must truncate the domain; we do this at $y = \pm 25$ with absorbing boundary conditions based on the background stress and velocity values (see Part 1 for more details).

There are two important situations that can arise for frictional sliding problems between elastic solids: one for which a steady state sliding solution exists and one for which a steady state sliding solution does not exist. For the steady state sliding solution, the fault continues to slide even after the

parameter	variable	value
Elastic Properties ($y \geq 0$)		
shear modulus	$G^{(1)}$	30.0
shear-wave speed	$c_s^{(1)}$	3.0
dilatational-wave speed	$c_p^{(1)}$	$\sqrt{3}\, c_s^{(1)}$
Elastic Properties ($y \leq 0$)		
shear modulus	$G^{(2)}$	24.3
shear-wave speed	$c_s^{(2)}$	2.7
dilatational-wave speed	$c_p^{(2)}$	$\sqrt{3}\, c_s^{(2)}$
Friction (Rate-and-State)		
state evolution distance	L	0.4
reference slip velocity	V_0	10^{-6}
direct effect parameter	a	0.016
Friction (Steady State)		
weakening velocity	V_w	0.17
evolution effect parameter	b	0.02
steady state friction at V_0	f_0	0.6
steady state friction at $V \gg V_0$	f_w	0.13
Initial Conditions		
background stresses	$\bar{\sigma}_{yx}^{(l)}$, $\bar{\sigma}_{yz}^{(l)}$	15 or 30 (see text)
	$\bar{\sigma}_{xx}^{(l)}$, $\bar{\sigma}_{zz}^{(l)}$	0
	$\bar{\sigma}_{yy}^{(l)}$	-126
background velocities	$\bar{v}_x^{(1)}$, $\bar{v}_z^{(1)}$	$+5 \times 10^{-17}$
	$\bar{v}_x^{(2)}$, $\bar{v}_z^{(2)}$	-5×10^{-17}
	$\bar{v}_y^{(l)}$	0

Table 1: Physical properties and parameters. These parameters are typical and of the right order of magnitude for real earthquake problems if the units are taken to be GPa for shear moduli, km/s for wave speeds, m/s for velocities, MPa for stresses, km for lengths, and m for displacements.

incident pulses have ceased interacting with the fault. In multiple dimensions, this results in what is knowns as the crack-like rupture mode, where once the rupture front passes a point on the fault it continues to slide until the arrival of outside information, such as waves arriving from the edge of the fault. When there is no steady state sliding solution the fault only slips for a finite amount of time and then locks. In multiple dimensions this results in the self-healing slip pulse rupture mode, where only a finite region of the fault is actively sliding near the rupture front. Self-healing slip pulses occur only for strongly velocity weakening steady state friction laws and for sufficiently low values of background shear stress [Zheng and Rice, 1998, Noda et al., 2009]. As indicated in Table 1 we test two different values for the background shear stress, $\bar{\sigma}_{yx}$ and $\bar{\sigma}_{yz}$, which give the two different solution types.

Before presenting the numerical results, we first explain the structure of the analytic solutions. In Figures 3 and 4 we present snapshots of the solution when a steady state sliding solution does and does not exist, respectively. For both sets of solution profiles the fault-normal velocity, v_y, remains continuous across the fault for all time, confirming the fact that the fault does remain closed, $w = 0$. Figures 3(a) and (e) clearly show the steady state sliding behavior with the higher background shear stress as the discontinuity in velocity across the fault remains after the wave packets have stopped interacting with the fault and the shear stress is also different than the background shear stress, Figures 3(b) and (f). Figures 4(a) and (e) do not show this behavior due to the lower background shear stress. Even though the initial wave packets are rather simple, both problems show complex final solutions.

Another important aspect of the solution is how the friction coefficient, $f(V, \Psi)$, evolves in time; Figure 5 shows the friction coefficient as a function of slip velocity and time for the initial conditions that allow for steady state sliding, (a) and (c), and the initial conditions that do not, (b) and (d), as well as the slip velocity as a function of time. From these plots several aspects of the problem can be understood. The rise in friction coefficient, label $\{1\}$, corresponds to the direct effect: an instantaneous increase in the friction coefficient accompanying an increase in slip velocity, as seen in Figure 1(a) and from (74) if ψ is held constant. After this $\{2\}$ the state variable begins to evolve causing weakening of the fault. Both of these effects are responses to the arrival of the z-polarized shear wave pulse and are followed by the direct effect during unloading $\{3\}$ as this pulse leaves the fault. The direct effect during loading $\{4\}$ and state evolution $\{5\}$ are caused by the x-polarized shear wave pulse. For the problem with higher background shear stress, (a)

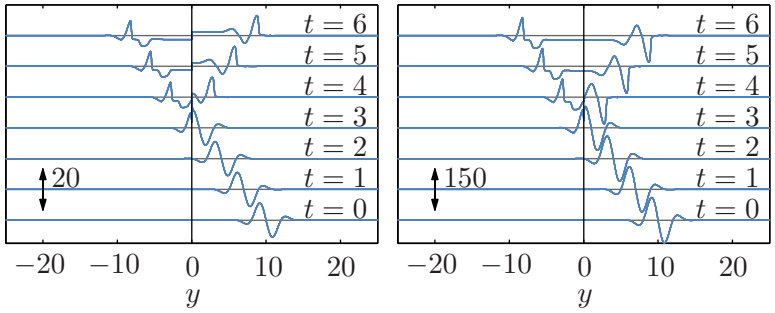

(a) v_x

(b) σ_{yx}

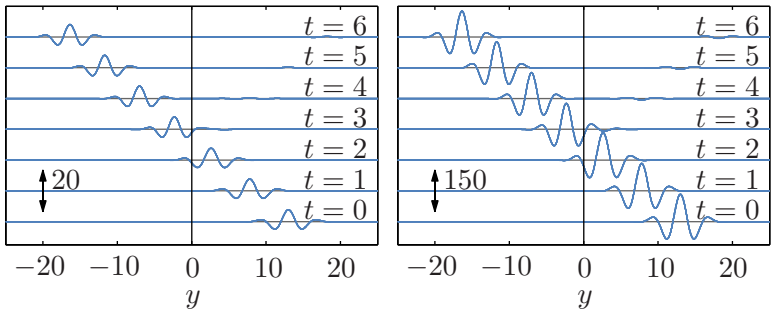

(c) v_y

(d) σ_{yy}

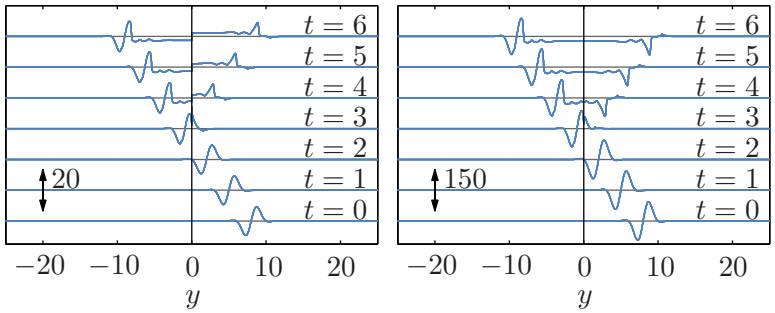

(e) v_z

(f) σ_{yz}

Figure 3: Exact solution with initial conditions ($\bar{\sigma}_{yx} = \bar{\sigma}_{yz} = 30$) for which a steady state sliding solution exists. As can be seen in (a) and (e) the fault continues to slide after the incident wave packets have stopped interacting with the fault. The gray line behind the blue solution profiles represents the background values.

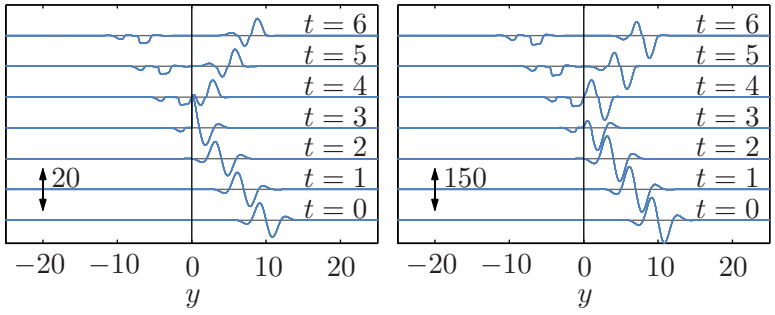

(a) v_x (b) σ_{yx}

(c) v_y (d) σ_{yy}

(e) v_z (f) σ_{yz}

Figure 4: Exact solution with initial conditions ($\bar{\sigma}_{yx} = \bar{\sigma}_{yz} = 15$) for which a steady state sliding solution does not exist. As can be seen in (a) and (e) the fault continues to slide after the incident wave packets have stopped interacting with the fault. The gray line behind the blue solution profiles represents the background values.

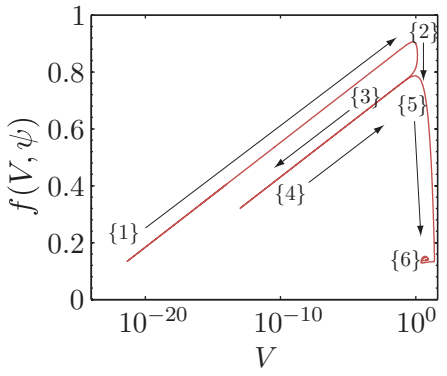

(a) Steady state sliding exists

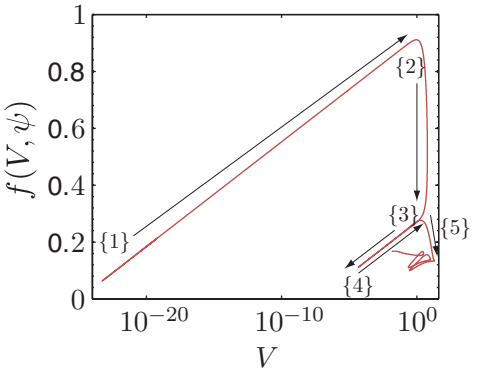

(b) Steady state sliding does not exist

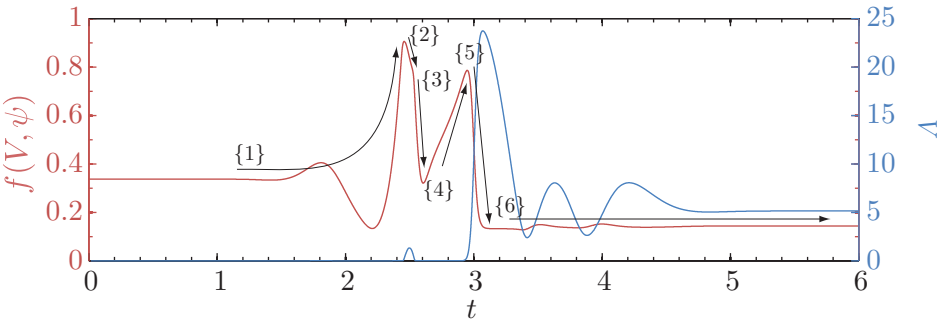

(c) Steady state sliding exists

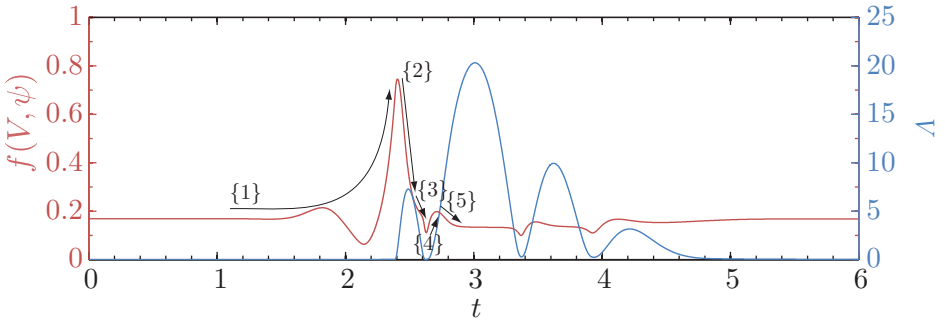

(d) Steady state sliding does not exist

Figure 5: Temporal evolution of the friction coefficient and slip velocity. Labels correspond to {1} direct effect (loading), {2} state evolution, {3} direct effect (unloading), {4} direct effect (loading), {5} state evolution, {6} steady state sliding in (a) and (c) (no steady state sliding in (b) and (d) with background conditions).

and (c), {6} corresponds to the steady state sliding behavior; this is not seen with the lower background stress values in (b) and (d), and the slip velocity would continue to evolve towards zero if the final times were increased.

We test both configurations with the developed numerical method using the 2^{nd}, 3^{rd}, and 4^{th} order diagonal norm SBP operators of Strand [1994] (order refers to the global accuracy and the interior accuracy of the methods is 2, 4, and 6 respectively). The time integration is carried out using the low memory, 4^{th} order Runge-Kutta method of Carpenter and Kennedy [1994], method 5[4] with solution 3, using a time step of $\Delta t = 0.9\ h/c_p$. Error is defined as using the energy norm (74):

$$\text{error}(N) = \|\boldsymbol{q}(\cdot, t_{end}) - \boldsymbol{q}(t_{end})\|_h, \tag{103}$$

where $\boldsymbol{q}(t)$ is the $2(N+1)$ grid point discrete solution ($N+1$ grid points on each side of the fault), and $\boldsymbol{q}(\cdot, t)$ is the exact solution (see (32)-(37)) evaluated at the grid points. The convergence rate is estimated using

$$\text{p}(N) = \log\left(\frac{\text{error}(N)}{\text{error}(2\ N)}\right) \Big/ \log\left(\frac{h(N)}{h(2\ N)}\right), \tag{104}$$

where $h(N) = 25/N$.

A plot of the error versus grid size is shown in Figure 6. As can be seen the method converges to the true solution, and as expected, the higher-order methods converge faster and to a lower final error for the same N. The convergence rate estimates are also shown and the methods approach their theoretical convergence rate with sufficient refinement.

5. Conclusions

This paper has considered the problem of a tensor elastic material with a rate-and-state frictional interface. A strictly stable discretization was developed using SBP difference operators with weak enforcement of the boundary conditions though the characteristic SAT method.

The characteristic SAT method uses the boundary conditions formulated in terms of the characteristic variables as opposed to the physical variables, which is necessary to avoid stiffness of the semi-discretized equations.

Two test problems were considered, one for which a steady state sliding solution exists and one for it does not. For both of these tests the method performed as expected resulting in high-order convergence. This is the first time that high-order convergence has been demonstrated for these earthquake-related problems with rate-and-state friction.

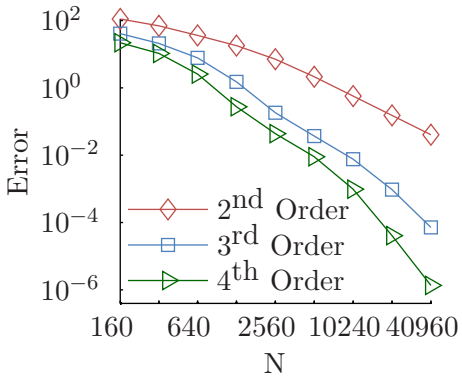

(a) Error: steady state exists

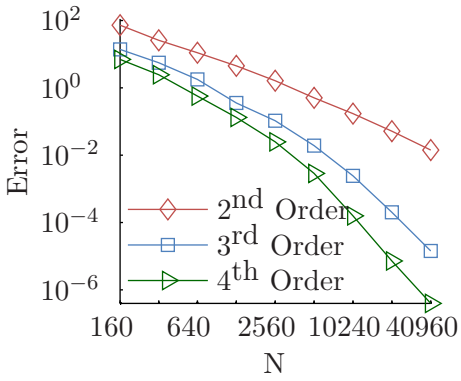

(b) Error: steady state does not exist

N	2^{nd}	3^{rd}	4^{th}
160	0.70	0.96	1.06
320	0.94	1.43	2.04
640	1.02	2.36	3.21
1280	1.34	3.05	2.66
2560	1.73	2.30	2.27
5120	1.91	2.29	3.21
10240	1.91	2.99	4.57
20480	1.89	3.73	4.91

(c) Rate: steady state exists

N	2^{nd}	3^{rd}	4^{th}
160	1.48	1.31	1.51
320	1.24	1.66	2.12
640	1.28	2.32	2.09
1280	1.47	1.75	2.41
2560	1.70	2.45	3.11
5120	1.56	2.97	4.19
10240	1.72	3.60	4.45
20480	1.87	3.81	4.18

(d) Rate: steady state does not exist

Figure 6: Error and convergence rate estimates for two test problems, one for which a steady state sliding solutions exists, and another for which it does not.

Acknowledgements

This research was supported by NSF-EAR award 0910574 and the Southern California Earthquake Center (SCEC), as funded by Cooperative Agreements NSF-EAR 0106924 and USGS 02HQAG0008 (SCEC contribution number 1424).

A. Bracketed Newton's Method for Nonlinear Friction Laws

Here we outline the bracketed Newton's method used to solve for $\boldsymbol{\mathcal{W}}^{+(1)}$ and $\boldsymbol{\mathcal{W}}^{-(2)}$ from $\boldsymbol{F}(\boldsymbol{V})$ with a two-sided fault and differing material properties; closed form solutions for $\boldsymbol{\mathcal{W}}^{+(1)}$ and $\boldsymbol{\mathcal{W}}^{+(2)}$ do not generally exist.

Throughout this appendix it is implied that the characteristic boundary conditions depend on the characteristic variables associated with stationary waves and waves propagating into the fault; see (23) and (24). The task is to find the characteristic boundary conditions by solving

$$\boldsymbol{\tau} = \boldsymbol{F}\left(\sigma_n, \boldsymbol{V}\right), \tag{105}$$

$$\boldsymbol{\tau} = \begin{bmatrix}\sigma_{xy}\\ \sigma_{zy}\end{bmatrix} = \frac{1}{2}\begin{bmatrix}w_{yx}^{-(1)} + \mathcal{W}_{yx}^{+(1)}\\ w_{yz}^{-(1)} + \mathcal{W}_{yz}^{+(1)}\end{bmatrix} = \frac{1}{2}\begin{bmatrix}\mathcal{W}_{yx}^{-(2)} + w_{yx}^{+(2)}\\ \mathcal{W}_{yz}^{-(2)} + w_{yz}^{+(2)}\end{bmatrix}, \tag{106}$$

$$\begin{aligned}\boldsymbol{V} &= \begin{bmatrix}v_x^{(1)} - v_x^{(2)}\\ v_z^{(1)} - v_z^{(2)}\end{bmatrix}\\ &= \frac{1}{2Z_s^{(1)}}\begin{bmatrix}w_{yx}^{-(1)} - \mathcal{W}_{yx}^{+(1)}\\ w_{yz}^{-(1)} - \mathcal{W}_{yz}^{+(1)}\end{bmatrix} - \frac{1}{2Z_s^{(2)}}\begin{bmatrix}w_{yx}^{-(2)} - \mathcal{W}_{yx}^{+(2)}\\ w_{yz}^{-(2)} - \mathcal{W}_{yz}^{+(2)}\end{bmatrix}.\end{aligned} \tag{107}$$

It is useful to combine (106) and (107) as

$$\boldsymbol{\tau} = \boldsymbol{\phi} - \frac{\tilde{Z}_s}{2}\boldsymbol{V}, \quad \boldsymbol{\phi} = \frac{\tilde{Z}_s}{2}\begin{bmatrix}\frac{w_{yx}^{-(1)}}{Z_s^{(1)}} + \frac{w_{yx}^{+(2)}}{Z_s^{(2)}}\\ \frac{w_{yz}^{-(1)}}{Z_s^{(1)}} + \frac{w_{yz}^{+(2)}}{Z_s^{(2)}}\end{bmatrix}, \tag{108}$$

where $\tilde{Z}_s$ is defined in (57). Note that $\boldsymbol{\phi}$ does not depend on the boundary condition, but only on the characteristic variables propagating into the fault. Now we must solve (108) along with the friction law (105) for $\boldsymbol{V}$ and $\boldsymbol{\tau}$. Once this is done, $\mathcal{W}_{yx}^{+(1)}$, $\mathcal{W}_{yz}^{+(1)}$, $\mathcal{W}_{yx}^{-(2)}$, and $\mathcal{W}_{yz}^{-(2)}$ can be found from (106).

In the text the assumption was made that $\boldsymbol{V}$ and $\boldsymbol{\tau}$ are parallel (55); thus from (108) it follows that $\boldsymbol{\phi}$ and $\boldsymbol{V}$ are parallel. Hence, we can solve (108) in two steps. First, find V by solving

$$\sigma_n f(V) = \phi - \frac{\tilde{Z}_s}{2}V, \tag{109}$$

where $\phi = \sqrt{\boldsymbol{\phi}^T\boldsymbol{\phi}}$, and then set $\boldsymbol{V} = V\frac{\boldsymbol{\phi}}{\phi}$ and $\boldsymbol{\tau} = \boldsymbol{F}(\sigma_n, \boldsymbol{V})$. The bracketed Newton's method outlined in Section 2.2 of Part 1 can be used to solve (109).

References

B. T. Aagaard, T. H. Heaton, and J. F. Hall. Dynamic earthquake ruptures in the presence of lithostatic normal stresses: Implications for friction models and heat production. *Bull. Seism. Soc. Am.*, 91(6):1765–1796, 2001. doi: 10.1785/0120000257.

J.-P. Ampuero. *Etude physique et numérique de la nucléation des séismes*. PhD thesis, Univ. Denis Diderot Paris, 2002.

D. J. Andrews. Rupture propagation with finite stress in antiplane strain. *J. Geophys. Res.*, 81(20):3575–3582, 1976.

D. J. Andrews. Dynamic plane-strain shear rupture with a slip-weakening friction law calculated by a boundary integral method. *Bull. Seism. Soc. Am.*, 75(1):1–21, 1985.

H. Aochi, E. Fukuyama, and M. Matsu'ura. Selectivity of spontaneous rupture propagation on a branched fault. *Geophys. Res. Lett.*, 27(22): 3635–3638, 2000.

N. M. Beeler, T. E. Tullis, and D. L. Goldsby. Constitutive relationships and physical basis of fault strength due to flash heating. *J. Geophys. Res.*, 113:01401, 2008.

M. H. Carpenter, D. Gottlieb, and S. Abarbanel. Time-stable boundary conditions for finite-difference schemes solving hyperbolic systems: Methodology and application to high-order compact schemes. *J. Comp. Phys.*, 111(2):220–236, 1994. doi: 10.1006/jcph.1994.1057.

M. H. Carpenter, J. Nordström, and D. Gottlieb. A stable and conservative interface treatment of arbitrary spatial accuracy. *J. Comp. Phys.*, 148(2): 341–365, 1999.

M.H. Carpenter and C.A. Kennedy. Fourth-order 2N-storage Runge-Kutta schemes. Technical Report NASA TM-109112, National Aeronautics and Space Administration, Langley Research Center, Hampton, VA, 1994.

A. Cochard and R. Madariaga. Dynamic faulting under rate-dependent friction. *Pure Appl. Geophys.*, 142(3):419–445, 1994. doi: 10.1007/BF00876049.

S. Das. A numerical method for determination of source time functions for general three-dimensional rupture propagation. *Geophys. J. Roy. Astr. Soc.*, 62(3):591–604, 1980. doi: 10.1111/j.1365-246X.1980.tb02593.x.

S. Das and B. V. Kostrov. An investigation of the complexity of the earthquake source time function using dynamic faulting models. *J. Geophys. Res.*, 93(B7):8035–8050, 1988.

S. M. Day. Three-dimensional finite difference simulation of fault dynamics: Rectangular faults with fixed rupture velocity. *Bull. Seism. Soc. Am.*, 72 (3):705–727, 1982.

S. M. Day, L. A. Dalguer, N. Lapusta, and Y. Liu. Comparison of finite difference and boundary integral solutions to three-dimensional spontaneous rupture. *J. Geophys. Res.*, 110:B12307, 2005. doi: 10.1029/2005JB003813.

J. de la Puente, J.-P. Ampuero, and M. Käser. Dynamic rupture modeling on unstructured meshes using a discontinuous Galerkin method. *J. Geophys. Res.*, 114:B10302, 2009. doi: 10.1029/2008JB006271.

J. H. Dieterich. Modeling of rock friction 1. Experimental results and constitutive equations. *J. Geophys. Res.*, 84(B5):2161–2168, 1979. doi: 10.1029/JB084iB05p02161.

G. Festa and J-.P. Vilotte. The Newmark scheme as velocity and stress time-staggering: an efficient PML implementation for spectral element simulations of elastodynamics. *Geophys. J. Int.*, 161(3):789–812, 2005. doi: 10.1111/j.1365-246X.2005.02601.x.

L. B. Freund. *Dynamic Fracture Mechanics*. Cambridge University Press, 1st edition, 1998.

P. H. Geubelle and J. R. Rice. A spectral method for three-dimensional elastodynamic fracture problems. *J. Mech. Phys. Solids*, 43(11):1791–1824, 1995. doi: 10.1016/0022-5096(95)00043-I.

B. Gustafsson. The convergence rate for difference approximations to mixed initial boundary value problems. *Math. Comp.*, 29(130):396–406, 1975.

B. Gustafsson, H.-O. Kreiss, and J. Oliger. *Time Dependent Problems and Difference Methods*. Wiley-Interscience, 1996.

T. Hirose and T. Shimamoto. Slip-weakening distance of faults during frictional melting as inferred from experimental and natural pseudotachylytes. *Bull. Seism. Soc. Am.*, 95(5):1666–1673, 2005. doi: 10.1785/0120040131.

Y. Ida. Cohesive force across the tip of a longitudinal shear crack and Griffith's specific surface energy. *J. Geophys. Res.*, 77:3796–3805, 1972.

N. Kame and T. Yamashita. Simulation of the spontaneous growth of a dynamic crack without constraints on the crack tip path. *Geophys. J. Int.*, 139(2):345–358, 1999. doi: 10.1046/j.1365-246x.1999.00940.x.

Y. Kaneko, N. Lapusta, and J.-P. Ampuero. Spectral element modeling of spontaneous earthquake rupture on rate and state faults: Effect of velocity-strengthening friction at shallow depths. *J. Geophys. Res.*, 113: B09317, 2008. doi: 10.1029/2007JB005553.

H.-O. Kreiss. Initial boundary value problems for hyperbolic systems. *Com. Pure Appl. Math.*, 23(3):277–298, 1970. doi: 10.1002/cpa.3160230304.

H.-O. Kreiss and G. Scherer. Finite element and finite difference methods for hyperbolic partial differential equations. In *Mathematical aspects of finite elements in partial differential equations; Proceedings of the Symposium*, pages 195–212, Madison, WI, 1974.

H.-O. Kreiss and G. Scherer. On the existence of energy estimates for difference approximations for hyperbolic systems. Technical report, Dept. of Scientific Computing, Uppsala University, 1977.

N. Lapusta, J. R. Rice, Y. Ben-Zion, and G. Zheng. Elastodynamic analysis for slow tectonic loading with spontaneous rupture episodes on faults with rate- and state-dependent friction. *J. Geophys. Res.*, 105:23765–23790, 2000.

S. Ma and P. Liu. Modeling of the perfectly matched layer absorbing boundaries and intrinsic attenuation in explicit Finite-Element methods. *Bull. Seism. Soc. Am.*, 96(5):1779–1794, 2006. doi: 10.1785/0120050219.

R. Madariaga, K. Olsen, and R. Archuleta. Modeling dynamic rupture in a 3D earthquake fault model. *Bull. Seism. Soc. Am.*, 88(5):1182–1197, 1998.

C Marone. Laboratory-derived friction laws and their application to seismic faulting. *Annu. Rev. Earth Planet Sci.*, 26(1):643–696, 1998. doi: 10.1146/annurev.earth.26.1.643.

K. Mattsson and J. Nordström. Summation by parts operators for finite difference approximations of second derivatives. *J. Comp. Phys.*, 199(2): 503–540, 2004. doi: 10.1016/j.jcp.2004.03.001.

T. Miyatake. Numerical simulations of earthquake source process by a three-dimensional crack model. part I. rupture process. *J. Phys. Earth*, 28(6): 565–598, 1980.

P. Moczo, J. Kristek, M. Gallis, P. Pazak, and M. Balazovjecha. The finite-difference and finite-element modeling of seismic wave propagation and earthquake motion. *Acta Phys. Slovaca*, 57(2):177–406, 2007.

S. Nielsen, G. Di Toro, T. Hirose, and T. Shimamoto. Frictional melt and seismic slip. *J. Geophys. Res.*, 113(B1):B01308, 2008. doi: 10.1029/2007JB005122.

H. Noda, E. M. Dunham, and J. R. Rice. Earthquake ruptures with thermal weakening and the operation of major faults at low overall stress levels. *J. Geophys. Res.*, 114:B07302, 2009. doi: 10.1029/2008JB006143.

J. Nordström. Conservative finite difference formulations, variable coefficients, energy estimates and artificial dissipation. *J. Sci. Comp.*, 29(3): 375–404, 2006. doi: 10.1007/s10915-005-9013-4.

J. Nordström. Error bounded schemes for time-dependent hyperbolic problems. *SIAM J. Sci. Comp.*, 30(1):46–59, 2007. doi: 10.1137/060654943.

J. Nordström and M. H. Carpenter. High-order finite difference methods, multidimensional linear problems, and curvilinear coordinates. *J. Comp. Phys.*, 173(1):149–174, 2001. doi: 10.1006/jcph.2001.6864.

D. D. Oglesby, R. J. Archuleta, and S. B. Nielsen. Earthquakes on dipping faults: The effects of broken symmetry. *Science*, 280(5366):1055–1059, 1998. doi: 10.1126/science.280.5366.1055.

P. Olsson. Summation by parts, projections, and stability. II. *Math. Comp.*, 64(212):1473–1493, 1995.

A. C. Palmer and J. R. Rice. The growth of slip surfaces in the progressive failure of over-consolidated clay. *Proc. Roy. Soc. London, Ser. A*, 332: 527–548, 1973.

G. Perrin, J. R. Rice, and G. Zheng. Self-healing slip pulse on a frictional surface. *J. Mech. Phys. Solids*, 43(9):1461–1495, 1995. doi: 10.1016/0022-5096(95)00036-I.

J. R. Rice. Constitutive relations for fault slip and earthquake instabilities. *Pure. Appl. Geophys.*, 121(3):443–475, 1983. doi: 10.1007/BF02590151.

J. R. Rice. Heating and weakening of faults during earthquake slip. *J. Geophys. Res.*, 111:05311, 2006.

J. R. Rice and A. L. Ruina. Stability of steady frictional slipping. *J. Appl. Mech.*, 50(2):343–349, 1983. doi: 10.1115/1.3167042.

J. R. Rice, N. Lapusta, and K. Ranjith. Rate and state dependent friction and the stability of sliding between elastically deformable solids. *J. Mech. Phys. Solids*, 49(9):1865–1898, 2001. doi: 10.1016/S0022-5096(01)00042-4.

O. Rojas, E. M. Dunham, S. M. Day, L. A. Dalguer, and J. E. Castillo. Finite difference modelling of rupture propagation with strong velocity-weakening friction. *Geophys. J. Int.*, 179:1831–1858, 2009. doi: 10.1111/j.1365-246X.2009.04387.x.

A. Ruina. Slip instability and state variable friction laws. *J. Geophys. Res.*, 88(B12):10,359–10,370, 1983.

W. S. Slaughter. *The Linearized Theory of Elasticity.* Birkhäuser, 2002.

B. Strand. Summation by parts for finite difference approximations for d/dx. *J. Comp. Phys.*, 110(1):47–67, 1994. doi: 10.1006/jcph.1994.1005.

M. Svärd and J. Nordström. On the order of accuracy for difference approximations of initial-boundary value problems. *J. Comp. Phys.*, 218(1): 333–352, 2007.

A. Tsutsumi and T. Shimamoto. High-velocity frictional properties of gabbro. *Geophys. Res. Lett.*, 24:699–702, 1997.

G. Zheng and J. R. Rice. Conditions under which velocity-weakening friction allows a self-healing versus a cracklike mode of rupture. *Bull. Seism. Soc. Am.*, 88(6):1466–1483, 1998.